



Project no. TIP5-CT-2006-031415

## INNOTRACK

Integrated Project (IP)

Thematic Priority 6: Sustainable Development, Global Change and Ecosystems

### D4.2.5 Improved model for the influence of vehicle conditions (wheel flats, speed, axle load) on the loading and subsequent deterioration of rails

Due date of deliverable: 2009-02-28

Actual submission date: 2009-02-28

Start date of project: 1 September 2006

Duration: 36 + 4 months

Organisation name of lead contractor for this deliverable:

Newcastle University

Revision [final]

Project co-funded by the European Commission within the Sixth Framework Programme (2002-2006)		
Dissemination Level		
PU	Public	X
PP	Restricted to other programme participants (including the Commission Services)	
RE	Restricted to a group specified by the consortium (including the Commission Services)	
CO	Confidential, only for members of the consortium (including the Commission Services)	

# Table of Contents

---

<b>Glossary .....</b>	<b>3</b>
<b>1. Executive Summary .....</b>	<b>4</b>
<b>2. Introduction .....</b>	<b>7</b>
<b>3. SUROS Tests .....</b>	<b>8</b>
3.1 Overview.....	8
3.2 Material data.....	8
3.3 Wear rates and traction coefficients .....	11
3.4 Hardness measurements .....	13
3.5 Strain estimates.....	16
<b>4. Wear-Hardness Correlation.....</b>	<b>18</b>
4.1 Literature review.....	18
4.2 Hardness analysis and discussion .....	22
4.3 Summary .....	24
<b>5. Wear modelling .....</b>	<b>26</b>
5.1 Development and calibration.....	26
5.1.1 Background.....	26
5.1.2 The model.....	26
5.1.3 Model calibration.....	28
5.2 Different vehicle characteristics.....	31
5.3 Summary .....	34
<b>6. Crack modelling .....</b>	<b>36</b>
6.1 OOR and contact stress-driven crack propagation .....	36
6.2 The effect of wheel flats on rail breaks.....	40
6.2.1 Methodology .....	40
6.2.2 Simulations .....	41
6.2.3 Conclusions .....	42
<b>7. Conclusions.....</b>	<b>43</b>
<b>8. Bibliography .....</b>	<b>45</b>
<b>9. Annexes .....</b>	<b>47</b>

## Glossary

---

<b>Abbreviation/acronym</b>	<b>Description</b>
OOR	Out-of-round
RCF	Rolling contact fatigue
SUROS Machine	<u>S</u> heffield <u>U</u> niversity <u>R</u> olling <u>S</u> liding [Twin-Disc Machine]
VAS	Voestalpine Schienen GmbH
SIF	Stress Intensity Factor

# 1. Executive Summary

---

The aim of this deliverable is an improved model for the influence of vehicle conditions on the loading and subsequent deterioration of rails. In particular, this report focuses on:

1. Wear data from SUROS twin-disc tests with CORUS 260 and premium grade pearlitic rail steels (CORUS 400, VA 350 and VA 400), and metallurgical analysis (micro-hardness and shear strain measurement) of section disc samples.
2. The effect of wheel hardness on rail wear rate, and vice versa: findings from the academic literature, and observations from InnoTrack SP4 SUROS twin-disc tests.
3. Development, calibration and validation of Newcastle University's wear and crack initiation model (dynarat, a.k.a. the 'brick' model):
  - a. development of material models for each of the tested rail steels;
  - b. calibration of the wear model against the results of the CORUS 260 dry tests; and
  - c. validation of the wear model against the results for the premium grade steels.
4. Wear modelling (using the calibrated wear model) of wheel-rail contact on top of the rail head, focussing on the effects of load and traction; develop a method for quickly estimating wear.
5. The effect of out-of-round (OOR) wheels on wear and crack initiation.

## **Wear-Hardness Correlation**

Four pearlitic rail steels were tested against VAS R7 wheel steel. Three twin-disc tests were performed for each rail steel: 5000 cycles dry; 5000 cycles dry followed by 5000 cycles wet (i.e., water-lubricated); and 15000 cycles dry.

In general, the harder the rail disc material becomes at the surface, the harder the wheel disc material becomes at the surface. Rail disc wear decreases when rail steel hardness increases. In wet tests, wheel disc wear rate drops as rail disc hardness increases. In the system as a whole (i.e., considering both wheel and rail discs), using harder CORUS 400 and VA 400 rail steels lowers the total wear rate.

From a review of the academic literature, there is no conclusive finding that harder rails wear wheels more, or vice versa. In general, harder materials wear less, but material hardness is not the only determining factor of wear performance; microstructure and strain-hardening behaviour are critical factors, and rolling contact fatigue performance is equally important. However, as a fairly general rule:

→ *To reduce system wear, harder steel grades should be used for both wheel and rail.*

## **Wear Model Development, Calibration and Validation**

The mixed (dry-wet) SUROS tests caused severe rolling contact fatigue, affecting hardness readings and wear rates, but the dry tests have provided an excellent resource for wear model development and calibration.

Test specimens have been sectioned and analysed. Microhardness measurements have suggested a possible softening effect at very small strains, and a new strain-hardening equation is used to fit to the strain-hardness data for each of the four steels. Wear model calibration has led to a number of core developments to the model itself.

The wear rate predictions for the premium grade rail steels match measured values (approximately) for the 5000 cycles dry tests, but over-predict the wear rate for the 15000 cycles dry tests by a factor of 2-3. (The dry-wet test predictions do not match, but are not expected to, since the ratcheting wear model does not account for major surface deterioration caused by significant surface cracking.)

→ *Following major development, the wear model has been calibrated successfully for CORUS 260 rail steel under dry contact conditions.*

→ *The wear model has been partly validated for the premium grades. Additional test work and metallurgical analysis should lead to improved material hardening models.*

## **Effect of Vehicle Characteristics: Rail Wear Predictions**

The wear model, calibrated for CORUS 260 and dry contact, was used to study the effect on rail wear of vehicle characteristics through their effect on the wheel-rail contact. The patch was assumed to be

elliptical and the pressure distribution to be Hertzian; in addition, the contact was assumed to be on the top the rail, suitable for straight track, not curves, and the traction to be longitudinal only.

Traction coefficient has a significant effect on the wear rate. For distributed traction systems the traction coefficient may often be about 0.1, i.e., an average wear rate of about 0.75nm/cycle. For locomotives the traction coefficient may be 0.3 or even higher, i.e., an average wear rate of 1.5nm/cycle or more.

- *There was a very clear linear trend of wear rate against peak contact pressure (for the range of pressures studied).*
- *Wear equations, giving wear rate for a given pressure and traction coefficient, have been extrapolated which can be used for quick estimation of rail wear.*

### **Out-of-Round Wheels**

The effect of pressure variation (with wavelengths above about 20mm) on rail wear rate was studied by considering each wheel pass as an independent event. Wear simulations were thus performed by varying the normal load with each passing wheel, and the predictions compared with the constant average-load case. No significant difference was observed.

- *Out-of-round pressure variations do not affect rail wear significantly.*

The effect of periodic variation of wheel-rail contact patch pressure on propagation of semi-circular cracks up to 12mm radius (i.e., penetrating to a depth of about 6mm at 30° angle to the surface) was studied using the '2.5D' Green's-function-based model. The following conclusions were reached:

- *For pressure variations with a wavelength less than about 2mm, the maximum pressure should be used to calculate crack growth rate.*
- *For pressure variations with a wavelength greater than about 20mm, there is no advantage to modelling pressure variation within a single load pass, and that modelling successive wheel passes with different static pressures would be sufficient.*
- *Out-of-round wheels with roughness features between these two wavelengths would accelerate crack propagation, but would require more detailed modelling.*

### **Rail crack growth and rail breaks**

For an analysis of long crack growth and rail breaks numerical simulations validated and calibrated towards full-scale field tests featuring flatted wheels have been employed. The main conclusions from the simulations were the detrimental influence of rail temperature and low ballast stiffness (where hanging sleeper(s) is an extreme case).

The influences of the most important parameters have been quantified. The results are presented in Annexes 4, 5 and 6 and summarized in Section 6.2. The main conclusions and operational recommendations are:

- *Critical crack sizes (i.e., crack sizes for which fracture is likely) for rail head and foot cracks depend significantly on the temperature (or rather the temperature below the stress free temperature). For cold conditions, critical crack sizes of roughly 1 and 3 cm are found for rail foot and rail head cracks respectively.*
- *Crack growth rates are significantly increased close to fracture. Consequently, operationally **allowed** crack sizes need to be much smaller. Exactly how much smaller depends on the accuracy of inspections (i.e., how small cracks can with certainty be detected) and inspection intervals. To guide in this decision, crack growths evaluated for different operational conditions and presented in Annex 6 can be employed.*
- *A decrease in the assured largest crack size after an inspection (i.e., the size of a crack that with full certainty can be found at an inspection) will have a major influence on the needed length of the inspection intervals.*
- *Low ballast stiffness will normally lead to higher rail bending moments. To avoid this influence the ballast stiffness per half sleeper should be kept above some 30 MN/m. Hanging sleepers will remove the beneficial effect of high ballast stiffness and should be avoided. In particular this seems to be the case for high-speed operations (200 km/h in the current study).*

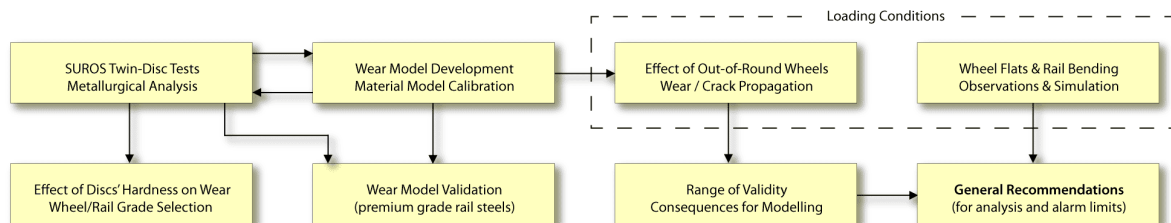
- *It is recommended to combine the mitigation of a hanging sleeper with an inspection for rail head and rail foot cracks.*
- *The temperature will have a very significant effect on both crack growth rates and risk of final fracture. To this end it is recommended that the magnitude of allowed wheel–rail impact forces be related to the temperature. Further, inspection intervals need to be significantly reduced during cold periods. Guidance in defining alarm limits and inspection intervals can be obtained from the results presented in Annex 6.*
- *Due to the significant increase in crack growth rates in cold climate, it is recommended that there is an inspection before a cold period to minimize the occurrence of larger cracks that may propagate to fracture.*
- *The wheel–rail impact force will have an effect on the risk of fracture. To establish alarm limits is a balance between allowed forces and allowed crack sizes. Due to this, a higher alarm limit can be allowed if shorter crack sizes are assured (e.g., by more frequent inspections).*
- *It is wise to introduce multiple alarm levels for several reasons:*
  - *A wheel that induces a high impact load is likely to cause damage on the vehicle (in the wheel, in the roller bearing, etc.). This may lead to increased costs and operational disturbances.*
  - *Also, wheels that induce impact loads below an alarm limit corresponding to rail breaks may cause smaller, arrested cracks to start growing. In particular, this is likely to be an issue for rail head cracks where a higher load may cause a crack to deviate transversally, which eventually may lead to a rail break.*
  - *The introduction of low-level alarms is likely to give the maintenance organisation improved possibilities of planning and optimising maintenance procedures. If only a one-level alarm exists there is an obvious risk that a vehicle that just passes the limit may fail in a subsequent control where operational conditions are slightly different. This will, obviously, result in unnecessary costs and operational disturbances.*
  - *For the same reason as outlined above, it is recommended that the low-level alarm limit is gradually decreased over a period before the introduction of “cold climate” alarm limits.*

## 2. Introduction

The primary objective of the work presented in this deliverable is to model various vehicle and wheel/rail material influences on wheel/rail degradation. This ties in with the overall objective of Work Package (WP) 4.2, which is to:

- define allowable tolerances for rail and joint geometry maintenance,
- establish minimum action rules for defects in rails and joints,
- establish inspection tolerances.

The research covered by this deliverable follows the basic plan outlined in this chart:



Section 3 has data obtained from SUROS twin-disc testing. During test runs, traction coefficient vs number of cycles is directly calculated. Wear of material discs is obtained from measuring weight and disc diameters prior to and after testing. Vickers hardness is measured on the disc cross-section under the centre of the contact. Deformation of material is observed in microscopic images of etched specimens, and strain is calculated against the depth from the disc surface.

Section 4 looks at the effect of counterface hardness on wear rate. This includes a literature survey of similar research and analysis of the current InnoTrack tests with different rail grades. This analysis will give input to derivation of minimum action rules for rails and guidelines on the effect of varying hardness on rail vs wheel.

Section 5 describes the development and calibration of the wear model, based on the SUROS test results, and looks at the effect of vehicle characteristics and variable loading on rail wear.

Section 6 looks at the effect of vehicle characteristics, particularly the effect of increased loading from out-of-round wheels. This includes:

- study of the effect of out-of-round loading on short crack propagation using the '2.5D' Green's-function-based model,
- study of the effect of out-of-round loading on large crack propagation.

## 3. SUROS Tests

---

### 3.1 Overview

A series of twin-disc tests has been performed for InnoTrack SP4/WP4.3 using the SUROS twin-disc test machine. SUROS machine is designed to simulate wheel-rail contact and rolling-sliding behaviour in the laboratory, to study wear of wheel and rail steels, plastic deformation, rolling contact fatigue (i.e., cracking), friction modifiers, track contaminants (e.g., sand, leaves) and isolation, and decarburization. A detailed laboratory report of the SUROS tests performed for the InnoTrack project is attached as Annex 1 and some additional analysis and reporting is presented in InnoTrack SP4/WP4.3 (see, e.g, Deliverable 4.3.3).

Tests were performed at contact pressure 1500MPa and slip -1% (to simulate a driving wheel), conditions which have been used extensively with the SUROS machine in the past. The disc diameter is about 47mm for both rail and wheel discs, which are machined from rail and wheel sections. Five different rail steels are to be tested: 260 grade, provided by Corus, and 350<sup>1</sup> and 400 grades, provided by Corus and Voestalpine. The wheel material is R7, provided by Voestalpine.

The following test sequences have been performed:

1. 5000 cycles dry (i.e., without water or other lubrication).
2. 5000 cycles dry, followed by 5000 cycles with water lubrication.
3. 15000 cycles dry.

### 3.2 Material data

The increased traffic and load on railways demands improved materials that will withstand the increase of stresses that lead to wear and cracking. These days, most steels used are pearlitic, with different hardness levels. Microstructure characteristics have an important influence on wear and RCF as well. Data on the Corus rail materials and VAS wheel material tested are presented in Table 1 and Table 2.

---

<sup>1</sup> Testing of Corus 350 grade has been delayed.

**Table 1.** *Material chemical analysis data.*

	<b>7TR19</b>	<b>7TR35</b>	<b>8TR76</b>	<b>8TR78</b>
<b>Manufacturer</b>	<b>Corus MSM</b>	<b>Corus HY</b>	<b>Corus HY</b>	<b>VAS</b>
<b>Grade</b>	<b>260</b>	<b>MHH400</b>	<b>350HT</b>	<b>R7 Wheel</b>
C	0.76	0.78	0.79	0.51
Si	0.26	0.62	0.43	0.34
Mn	1.03	0.91	1.13	0.74
P	0.015	0.016	0.012	0.011
S	0.02	0.014	0.019	0.006
Cr	0.02	0.51	0.02	0.24
Mo	0.005	0.005	0.005	0.005
Ni	0.02	0.03	0.02	0.02
Cu	0.01	<.01	0.01	0.05
Sn	<.005	<.005	<.005	<.005
Al	0.004	0.003	0.003	0.028
As	<.005	<.005	<.005	0.005
B	0.0005	<.0005	<.0005	<.0005
Ca	<.0005	<.0005	<.0005	0.001
Co	0.004	0.005	0.004	0.003
N	0.0046	0.005	0.005	0.005
Nb	0.001	0.001	0.001	0.001
Sb	0.0005	0.0005	0.0005	0.001
Ti	0.0003	0.012	0.0004	0.0017
V	0.001	0.002	0.001	0.001
W	0.001	0.001	0.001	0.001

**Table 2.** *Grade comparison.*

	<b>UTS(MPa)</b>	<b>0.2% Proof (MPa)</b>	<b>Elongation(%)</b>	<b>Running surface Hardness Brinell</b>
<b>260</b>	962	514	11	277
	983	580	10	276
	966	535	10	271
	980	521	12	293
	977	521	11	267
<b>400MHH</b>	1315		13	388
	1296		13	394
	1335		12.2	401
	1341		12.2	401
	1347		12.4	398
	1357		12.2	398
<b>R350HT</b>	1210	763	12	360

Material microstructure images are obtained by optical microscope and shown in Figure 1- Figure 5. Images are taken from discs tested for 5000 cycles dry, 10mm under the running surface, because material deformation should not have had a *visible* effect at this depth.

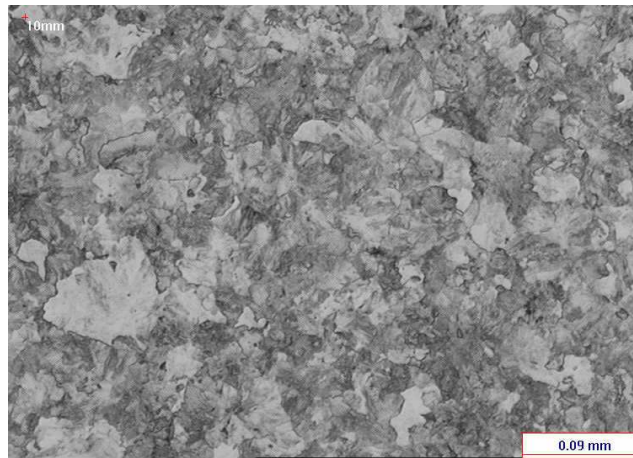


**Figure 1** *Optical microscope image, rail disc INR1, material CORUS 400 grade, 10mm under the surface. Test INNOT-01, 5000 cycles dry.*



**Figure 2** *Optical microscope image, rail disc INR10, material VA 350 grade, 10mm under the surface. Test INNOT-04, 5000 cycles dry.*

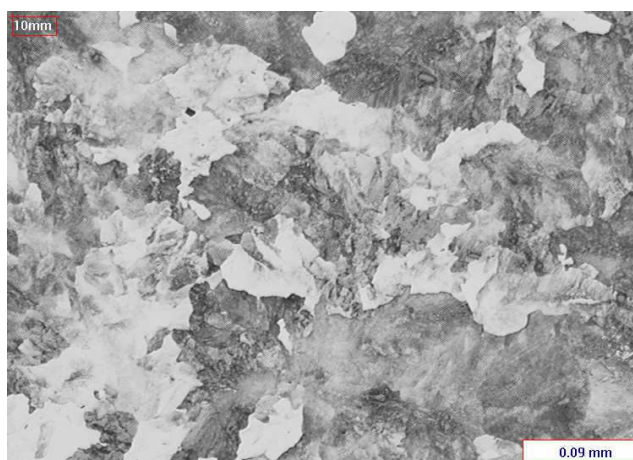


**Figure 3** *Optical microscope image, rail disc INR24, material CORUS 260 grade, 10mm under the surface. Test INNOT-07, 5000 cycles dry.*

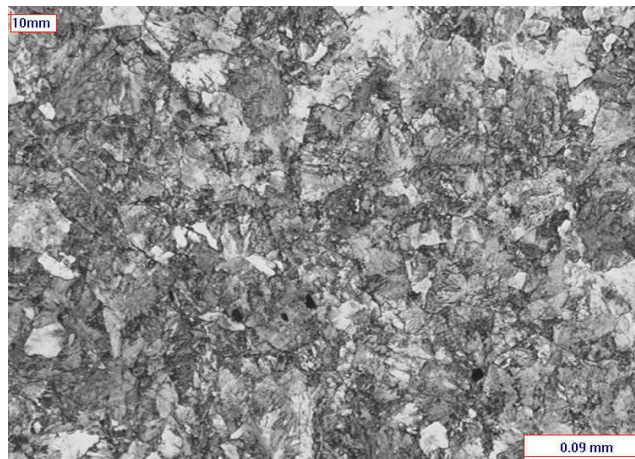


**Figure 4** *Optical microscope image, rail disc VA400(1), material VA 400 grade, 10mm under the surface. Test INNOT-010, 5000 cycles dry.*

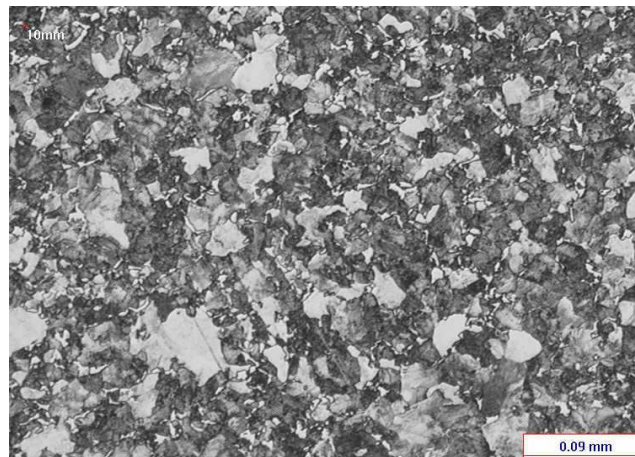


**Figure 5** *Optical microscope image, wheel disc INW1, material VAS R7, 10mm under the surface. Test INNOT-01 5000 cycles dry, against rail disc material CORUS 400.*

### 3.3 Wear rates and traction coefficients

Wear rates (based on mass-loss measurements and converted to average depth of material removed per cycle) are summarized in Table 3 for the CORUS 260 and 400 grades and the VA 350 and 400 grades. Traction coefficients for the first 5000 cycles (dry), averaged over three tests, are presented in Figure 6 for each of the four materials, along with the traction coefficient for the 5000 cycles water-lubricated (wet). The four rail steels have similar performance with regards to traction coefficient under these conditions.

**Table 3.** Summary of rail and wheel disc wear rates in InnoTrack SUROS twin-disc tests.

Steel Density

7.95 [g/cm3]

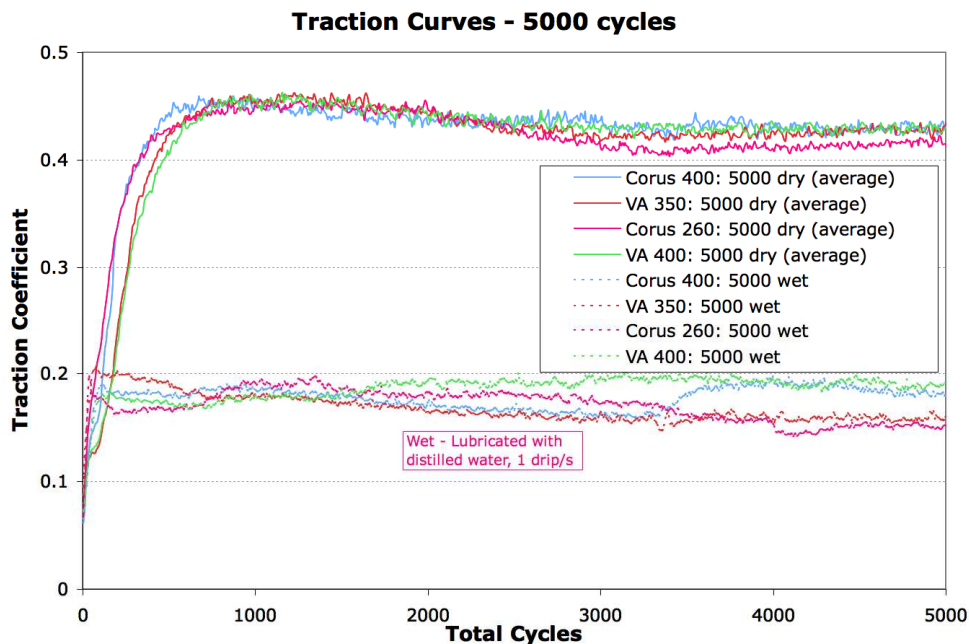
Track Width

10 [mm]

Test Name	Test ID	Rail Disc Material	Lubrication	[mm] Diameter	#Cycles	[g] Original Mass	[g] Final Mass	[g] Mass Loss	[µg/cycle] Wear Rate	[nm/cycle] Wear Rate
INN-01	C400-5000	CORUS 400	Dry	46.97	5013	180.3178	180.3054	0.0124	2.474	0.211
INN-02 a	C400-10000	CORUS 400	Dry	46.99	5013	180.4118	180.3979	0.0139	2.773	0.236
INN-02 b	C400-10000	CORUS 400	Wet	46.99	5016	180.3979	180.3506	0.0473	9.430	0.803
INN-03	C400-15000	CORUS 400	Dry	47	15014	180.1083	180.0715	0.0368	2.451	0.209
INN-04	V350-5000	VA 350	Dry	46.98	5011	180.6997	180.6741	0.0256	5.109	0.435
INN-05 a	V350-10000	VA 350	Dry	46.99	5014	180.4083	180.392	0.0163	3.251	0.277
INN-05 b	V350-10000	VA 350	Wet	46.98	5013	180.392	180.3861	0.0059	1.177	0.100
INN-06	V350-15000	VA 350	Dry	47	15014	180.3917	180.315	0.0767	5.109	0.435
INN-07	P260-5000	CORUS 260	Dry	46.98	5014	180.5581	180.5271	0.031	6.183	0.527
INN-08 a	P260-10000	CORUS 260	Dry	46.97	5014	180.7453	180.7166	0.0287	5.724	0.488
INN-08 b	P260-10000	CORUS 260	Wet	46.97	5010	180.7166	180.4612	0.2554	50.978	4.346
INN-09	P260-15000	CORUS 260	Dry	46.98	15015	181.2587	181.0745	0.1842	12.268	1.046
INN-10	V400-5000	VA 400	Dry	46.99	5011	180.4915	180.4818	0.0097	1.936	0.165
INN-12a	V400-10000	VA 400	Dry	46.99	5013	180.5027	180.4879	0.0148	2.952	0.252
INN-12b	V400-10000	VA 400	Wet	47	5012	180.4879	180.4752	0.0127	2.534	0.216
INN-11	V400-15000	VA 400	Dry	47	15011	180.7681	180.7348	0.0333	2.218	0.189

Test	Wheel Disc Material	Lubrication	[mm] Diameter	#Cycles	[g] Original Mass	[g] Final Mass	[g] Mass Loss	[µg/cycle] Wear Rate	[nm/cycle] Wear Rate	
INN-01	C400-5000	VAS R7	Dry	46.96	5065	181.0489	181.0230	0.0259	5.114	0.436
INN-02 a	C400-10000	VAS R7	Dry	46.98	5066	180.8339	180.8051	0.0288	5.685	0.485
INN-02 b	C400-10000	VAS R7	Wet	46.96	5069	180.8051	180.8010	0.0041	0.809	0.069
INN-03	C400-15000	VAS R7	Dry	46.99	15169	180.9945	180.8929	0.1016	6.698	0.571
INN-04	V350-5000	VAS R7	Dry	47.01	5059	180.224	180.1879	0.0361	7.136	0.608
INN-05 a	V350-10000	VAS R7	Dry	47	5064	181.3028	181.279	0.0238	4.700	0.400
INN-05 b	V350-10000	VAS R7	Wet	46.96	5066	181.279	181.2718	0.0072	1.421	0.121
INN-06	V350-15000	VAS R7	Dry	47	15165	180.9953	180.8197	0.1756	11.579	0.986
INN-07	P260-5000	VAS R7	Dry	46.99	5063	181.1096	181.0855	0.0241	4.760	0.406
INN-08 a	P260-10000	VAS R7	Dry	46.99	5062	180.9138	180.9016	0.0122	2.410	0.205
INN-08 b	P260-10000	VAS R7	Wet	46.98	5060	180.9016	180.8819	0.0197	3.893	0.332
INN-09	P260-15000	VAS R7	Dry	46.99	15163	181.0548	180.9018	0.153	10.090	0.860
INN-10	V400-5000	VAS R7	Dry	46.99	5062	180.9727	180.9467	0.026	5.136	0.438
INN-12a	V400-10000	VAS R7	Dry	47	5062	180.9348	180.9063	0.0285	5.630	0.480
INN-12b	V400-10000	VAS R7	Wet	46.98	5061	180.9063	180.9034	0.0029	0.573	0.049
INN-11	V400-15000	VAS R7	Dry	46.99	15166	180.8324	180.7228	0.1096	7.227	0.616



**Figure 6** Traction coefficients for dry and wet contact for each of the four rail materials. The dry test values are averaged at each time index over the two 5000-cycle dry tests and the first 5000 cycles of the 15000-cycle dry test. The wet tests followed 5000 cycles dry.

### 3.4 Hardness measurements

Bulk/core hardness measurements for each test disc are given in Table 4.

Test specimens have been sectioned and microhardness measurements taken at different depths on a circumferential cross-section. The rail disc microhardness data are plotted in Figure 7-Figure 9, and are tabulated in Annex 1. (Note: A load of 200g was used for measuring Vickers microhardness of materials CORUS 260, CORUS 400 and VA 350, and corresponding wheel discs, and a load of 300g for VA 400, and corresponding wheel discs.) Two hardness measurements are taken at each depth under disc surface, except at depths of 1mm and 5mm, where four were taken. Values shown in Figure 7-Figure 9 are averages of the readings at each depth.

Microhardness measurements of the wheel discs from the twin-disc tests are given in Figure 10.

All discs have shown material hardening characteristics at the surface. The rail material hardens more when run for more cycles. The softer CORUS 260 steel hardens more at the surface (i.e., at a depth of 50 microns) than the harder VA 350 and CORUS 400 in dry tests, while the other two materials have similar hardening rates. In wet tests, the CORUS 260 deteriorated a lot and is almost always softer than the other two materials when measured from the surface into the depth of material.

The wheel discs had similar hardness values initially. When microhardness was measured after testing, the wheel discs (like the rail discs) had hardened most for 15000 cycles, less for 10000 cycles (5000 dry + 5000 wet), and the least for 5000 cycles dry. After 15000 cycles dry, the wheel disc microhardness at depth 50 microns correlates with the rail disc microhardness at depth 50 microns, i.e., the CORUS 260 was the hardest at this depth, then the VA 350, and finally the CORUS 400 and VA 400, and the corresponding wheel discs matched this order of hardness. However, there is no matching trend after 5000 cycles.

**Table 4.** Bulk hardness – HV10 (10kg load) – average of 2-3 measurements. Also, for comparison, average wear rates (dry only).

Corus 400 grade	Rail hardness [HV]	Rail wear rate [nm/cycle]	Wheel hardness [HV]	Wheel wear rate [nm/cycle]
5000 dry	295.33	0.211	215	0.436
5000 dry + 5000 wet	354		206	
15000 dry	378	0.209	238	0.571
<b>VA 350</b>	<b>rail</b>		<b>wheel</b>	
5000 dry	373	0.435	225	0.608
5000 dry + 5000 wet	388.5		211	
15000 dry	374.5	0.435	216.5	0.986
<b>Corus 260 grade</b>	<b>rail</b>		<b>wheel</b>	
5000 dry	276.5	0.527	202.5	0.406
5000 dry + 5000 wet	283		235	
15000 dry	258	1.046	217	0.860
<b>VA 400</b>	<b>rail</b>		<b>wheel</b>	
5000 dry	326	0.165	233	0.438
5000 dry + 5000 wet	329		201	
15000 dry	322	0.189	235	0.616

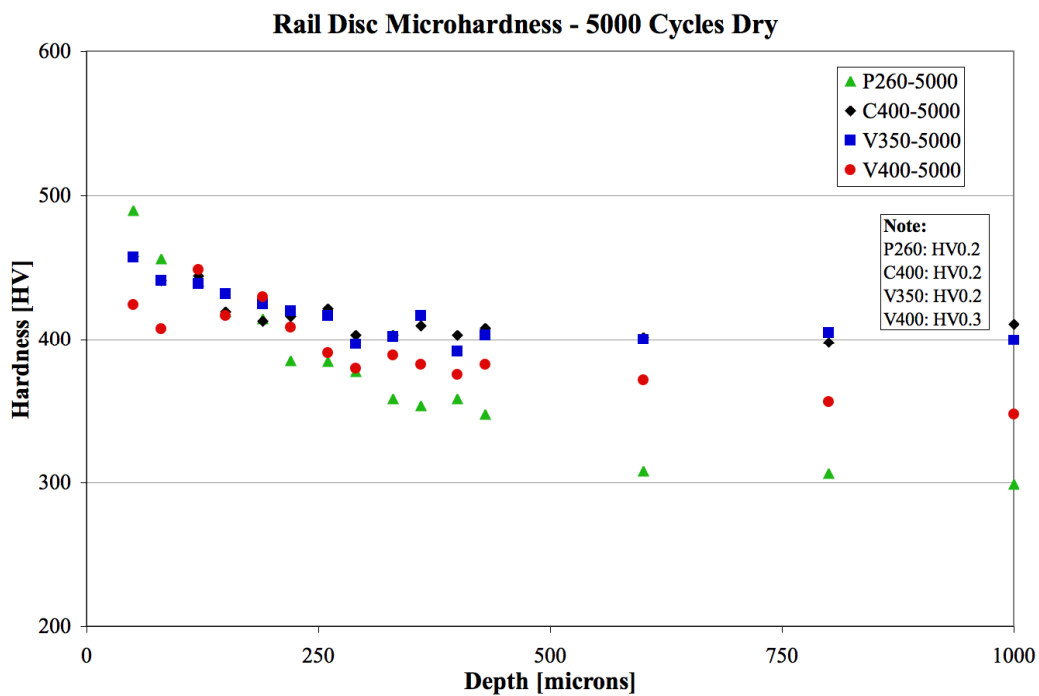


**Figure 7** Microhardness measurements at various depths on circumferential cross-sections through rail disc specimens following 5000 cycles dry.

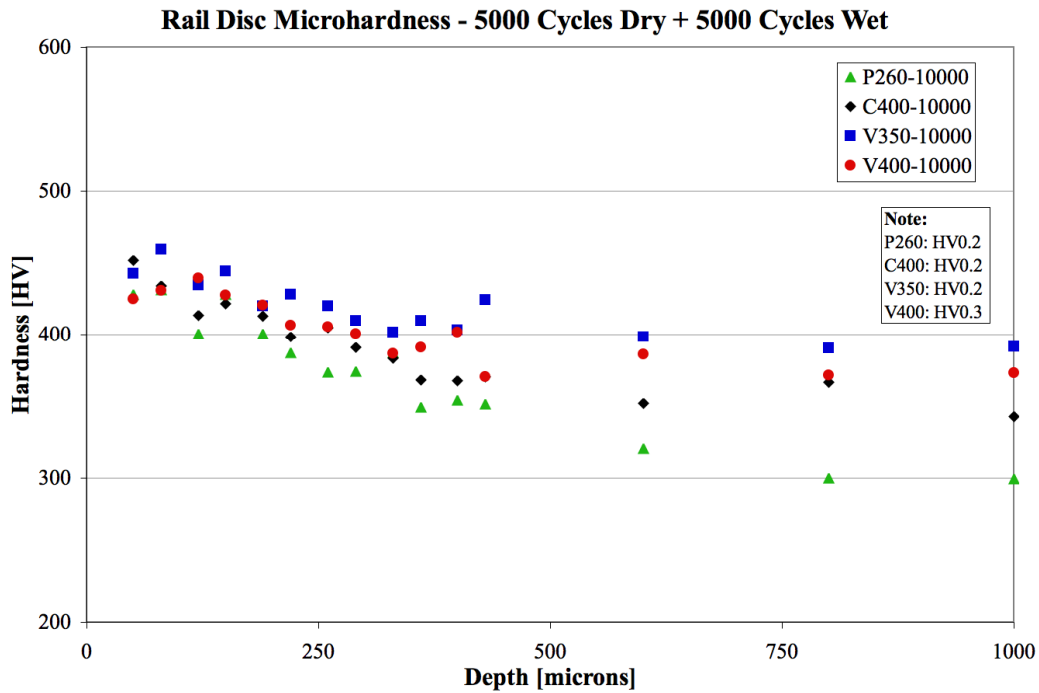


**Figure 8** Microhardness measurements at various depths on circumferential cross-sections through rail disc specimens following 5000 cycles dry and 5000 cycles wet.

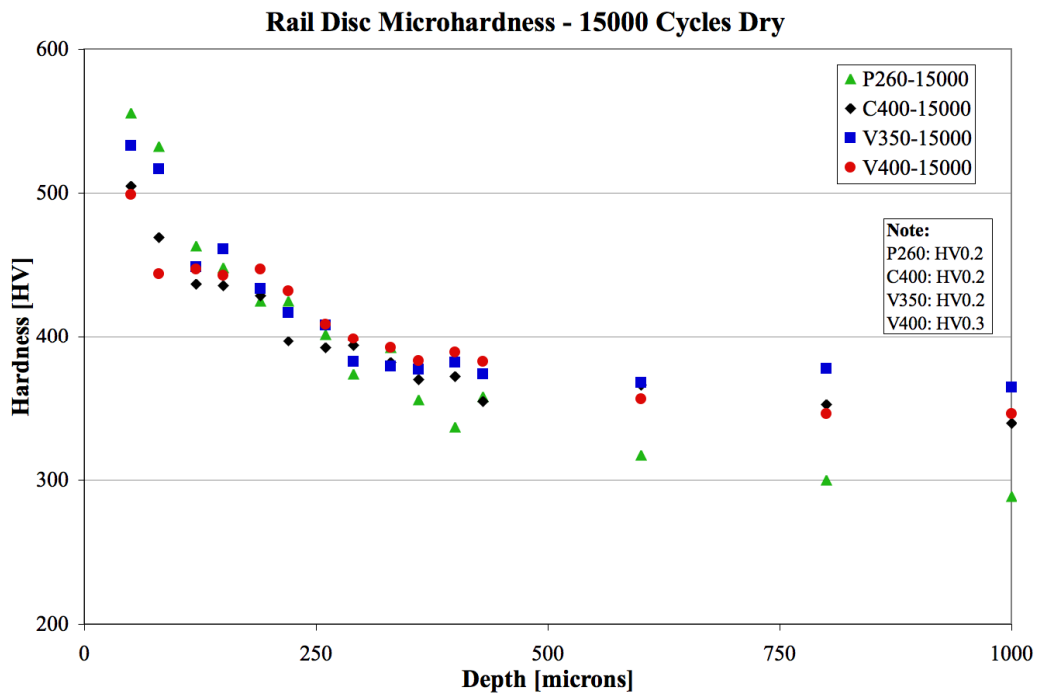


**Figure 9** Microhardness measurements at various depths on circumferential cross-sections through rail disc specimens following 15000 cycles dry.

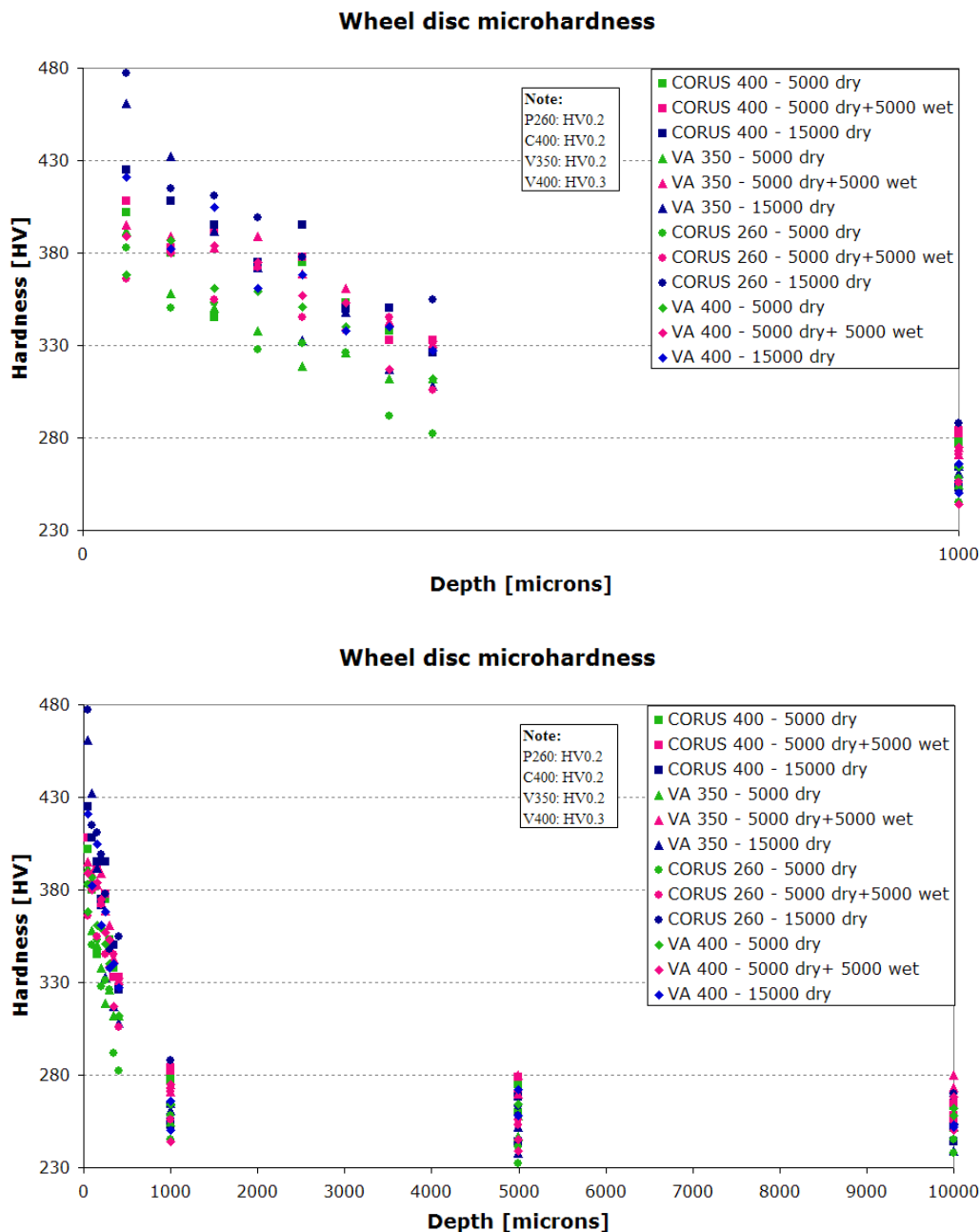


**Figure 10** Microhardness measurements at various depths on circumferential cross-sections through wheel disc specimens for all tests.

### 3.5 Strain estimates

#### Strain readings from optical microscope images

Tractive rolling, especially when unlubricated, causes very high levels of plastic shear strain to accumulate in rail steel. This shear strain is apparent in micrographs of sections of rail and twin-disc specimens through the distortion of the microstructure and the paths of near-surface cracks (see Annex 1).

To measure shear strain as objectively as possible, the microscope image is inputted in AutoCad. Lines were drawn following material strain lines (where these were visible), and angles and depths were measured (see Figure 11). In some cases, the image had to be rotated by up to three degrees, because the surface 0-line did not match perfectly the surface of the specimen (it is round and

cracked). Calculation of mean strain at each depth under surface was done by averaging strain angles for each depth first and then calculating shear strain. Measured shear strains for the four investigated rail materials are presented in Figure 12. Additional optical microscope images of cross-sections of tested rail discs are given in Annex 1.

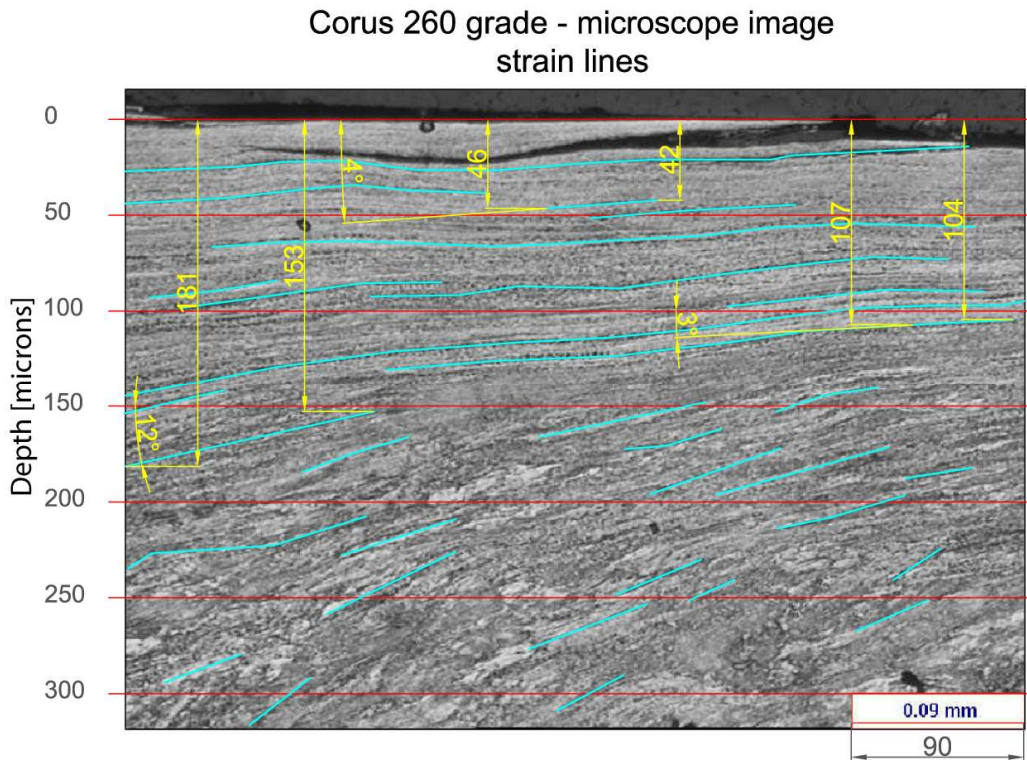


**Figure 11** Microscope image of Corus 260 grade steel. Drawn lines follow material strain lines. Some depths and angles are presented for interpretation of data reading method.

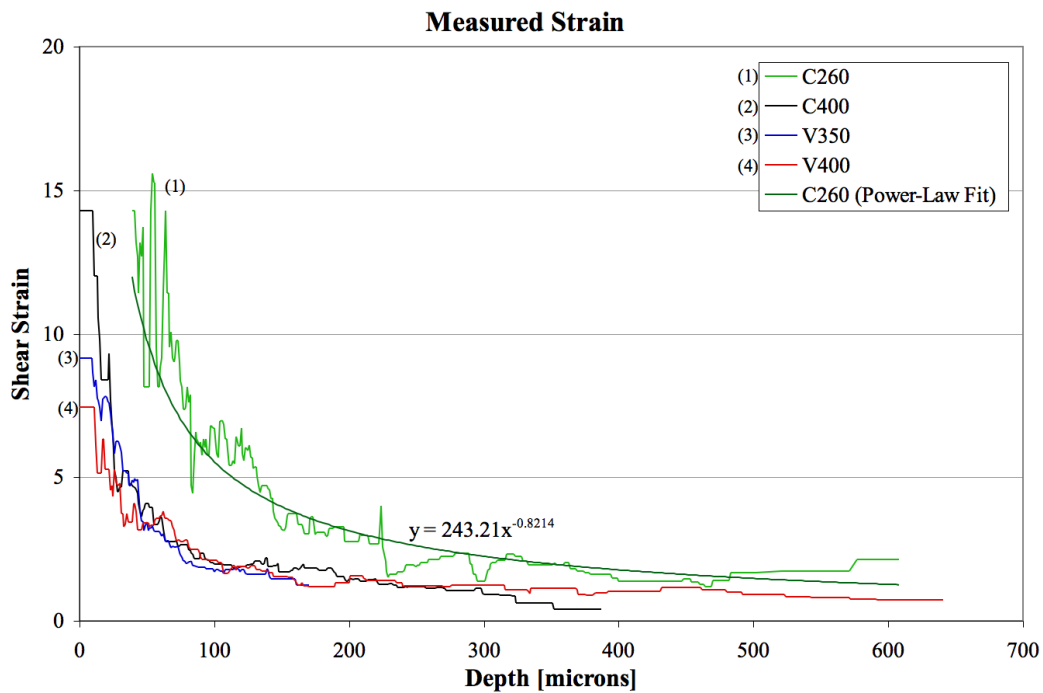


**Figure 12** Measured strain vs depth.

## 4. Wear-Hardness Correlation

### 4.1 Literature review

The influence of wheel hardness on rail wear rate, and vice versa, is not as widely researched as the influence of rail hardness on its own wear rate. Wheel hardness and rail hardness and their influence on wear are best studied as a system. It is difficult to compare results in the literature from modelling and from track tests and laboratory tests. Each researcher uses a slightly different method to calculate wear, and materials vary too.

Results obtained from research in the past show that there is not a straightforward dependence, because it is influenced by many other factors like contact load, slippage, direction of motion and material microstructure and chemical composition, i.e., interlamellar spacing and carbon content.

Dependence of rail hardness and wear, when wheel hardness is kept constant is shown in Figure 13. Both rail and system wear decrease as rail hardness increases (Pointner, 2008). Wheel wear, however, will at first increase for softer rails and, when using harder rails, it will remain constant.

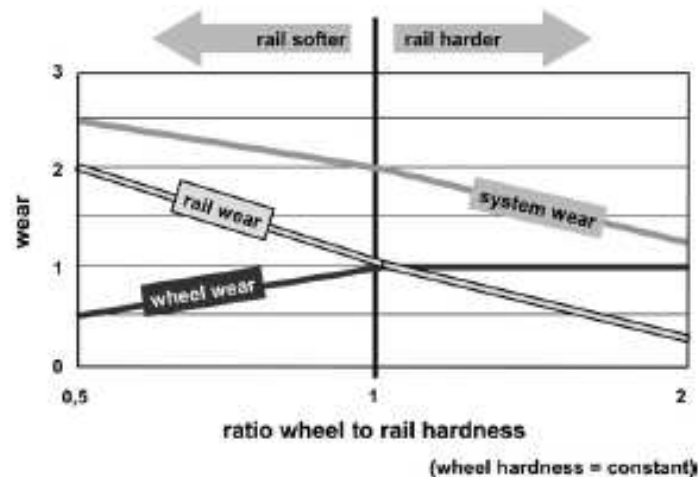


**Figure 13** Wheel, rail and system wear as a function of rail hardness; wheel hardness is kept constant (from Pointner, 2008).

Regarding wear resistance of material, the hardness of steel is closely connected to its microstructure. Research by Lee and Polycarpou (2005) shows that harder bainitic steels (J6) had worse wear performance in traffic than pearlitic steels, in contradiction to Archard's wear law (Archard, 1953; Jendel, 2002). This was connected to work hardening, where pearlitic steels hardened more. Hardness measurements were taken in detail on rail samples taken from new rail, from the low rail of a test track after 50 MGT, and from the high rail after 500 MGT. Cross-section SEM images of rail samples confirm findings from micro hardness Vickers tests, where the plastically deformed layer of J6 is only 70µm and clearly visible from the undeformed layer, while there is no definite layer formation of distinct plastic deformation in pearlitic rail samples. J6 showed improved RCF in service compared to pearlitic steels, because of the absence of surface and near surface microcracks. As an indication of core hardness of materials, new pearlite rail had 38.52HRC and new J6 bainite had 41.65HRC. Although, this research did not present wheel wear behaviour, it gives good guidance for choosing optimal rail/wheel material, working in a system, showing that relying on initial material hardness is not reliable for predicting wear rate, but steel work microhardening during operation has to be considered.

Strain-hardening behaviour of pearlitic rail steels was also observed by Tyfour et al. (1995). They performed twin-disc tests with W8A wheel material (275HV) for the driving disc, and BS11 rail material (240HV) for the driven disc. Contact pressure was 1500MPa and creepage of -1% in all dry air-cooled tests. Wear rates of both discs, in an experiment run for 40000 cycles, where the test was stopped every 2500 cycles for weight measurements, is shown in Figure 14. For the lower number of cycles wheel wear is slightly lower than rail wear and then increases significantly. The strain hardening of the pearlite steel in the rail disc specimen was at the maximum at the contact surface, 2.5 times higher

that of the bulk material. It was also noted that most of the hardening is achieved during the first stages of rolling cycles.

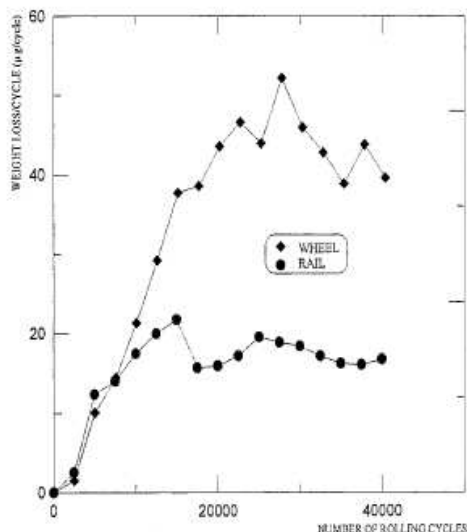


**Figure 14** A comparison between the wear rates of the rail and wheel test discs for test 130.

A series of laboratory twin-disc tests were conducted on Amsler-type testing machines by Markov (1995) with the aim of investigating the influence of wheel/rail hardness on wear rate. Test specimens were discs machined from rail heads and wheel rims, 40 mm in diameter and 6 mm in contact width. To achieve different hardness values, discs were oil quenched and tempered.<sup>2</sup> Test conditions, like contact pressure and slippage, were adjusted to resemble conditions on railway track, and so four test methods were used: rolling-sliding friction with longitudinal slippage, rolling-sliding friction with constant friction force, rolling-sliding friction with lateral slippage, and pure sliding friction. Wear rate ( $W$ ) was calculated as the difference of disc radius ( $\Delta r$ ) per revolution ( $n$ ):

$$W = \Delta r / n$$

and presented in units of millimetres per revolution. Mass loss measurements were used to correct decrease in radius. Discs were cleaned in ethanol before testing to remove any contamination. Tests were performed with no lubrication (dry).

The first set of tests simulated rolling-sliding friction with constant longitudinal slippage of -10%, with load 700 N so the maximum contact pressure was 650 N/mm<sup>2</sup>. The hardness of the rail rollers did not change and was 370 HV<sub>10</sub> in all experiments, while the hardness of the wheel rollers changed from 250 to 850 HV. Wear rates of wheel and rail discs were calculated after 70000 revolutions. Experiments showed that the wear rate of the rail disc is influenced by the change of hardness of the wheel disc and increases when wheel hardness increases, while the wear rate of the wheel disc decreases.

Markov (1995) presented results from tests with constant friction force that were originally conducted by Larin in 1958-1965, in order to simulate locomotive rim wear. The moment of friction force and the friction coefficient were constant and in the first set of tests were: moment 400-450 Ncm, friction coefficient 0.27-0.30, maximum contact pressure 537 N/mm<sup>2</sup>, and in the second set of tests moment 300-350 Ncm, friction coefficient 0.19-0.23, maximum contact pressure 619 N/mm<sup>2</sup>. Tests were run for 50000 revolutions and wheel and rail roller hardness were varied. Both sets of tests showed that when hardness of a roller increases, its own wear rate decreases, but its hardness also influences the wear rate of the opposite "counter-roller", which increases. The sum of the wear rates of both rollers was not sensitive to rail or wheel hardness.

Tests with constant lateral slippage of 5% were conducted for 70000 revolutions, with a maximum contact pressure of 950 N/mm<sup>2</sup>. The same conclusion can be derived as from previous tests. The

<sup>2</sup> This kind of heat treatment is very uncommon for wheels. The disadvantage consists in changing the microstructure also in an uncommon way because of producing a quenched and tempered microstructure instead of a fine-pearlitic microstructure. Therefore the results do not represent the practice at all.

wear rate of a roller is related directly to the hardness of the counter-roller, and inversely proportional to its own hardness. The hardness of both discs show only small influence on the total wear rate.

Tests with pure sliding friction were done as simulation of flats on a wheel tread and the process is also similar to side wear at the gauge face of rails. The top rail roller was fixed so slippage was -100%, and the speed of the bottom roller was 100 rev/min. Tests were run for only 300 revolutions under an initial pressure of 600 N/mm<sup>2</sup>. It was found that the wear rate of the top rail roller is 10 times higher than of the bottom wheel roller and that the wear rate of the top roller decreased with an increase of the hardness of either disc. In these experiments the influence of the hardness of the rail roller on the wear rate of the bottom wheel roller was negligible, but dependant on its own hardness. As the hardness of the wheel roller increased, its wear rate decreased.

The general conclusion by Markov (1995) is that the relationship between hardness and wear varies with different test conditions. In most of the experiments that were taken, rail wear rate depends on wheel hardness and it gets higher with harder wheels. Slippage has to be considered too. When components work under slippage less than 5%, wear rate redistributes according to disc hardness but total wear remains almost the same. It is recommended to increase rail/wheel hardness to reduce wear rate if they work under higher slippages.

The effect of varying wheel/rail material hardness on wear behaviour was investigated by Singh and Singh (1993) using laboratory experiments on an Amsler twin-disc machine and a pin-on-disc machine. Rolling-sliding twin-disc Amsler test disc specimens were machined from three types of rail (235HB, 278HB and 322HB) and one wheel (227HB) and were 40 mm in diameter and the contact width was 10mm. The wheel disc was the driving specimen and the rail disc was the driven specimen. Tests were run dry for one hour with 10% slip, under contact pressures of 312 N/mm<sup>2</sup>, 492 N/mm<sup>2</sup> and 696 N/mm<sup>2</sup>, at two different speeds of 200 and 400 r.p.m. During test runs, wear debris was continuously removed with a woollen cloth. The wear rate was calculated as the ratio of loss of mass of a disc to total rolling distance, in µg/m. Comparing the wear of just the rail disc shows an increase of wear with an increase of rolling speed and contact pressure, and a decrease in wear with an increase of material hardness. In all experiments the wheel disc was wearing more than the rail disc. The wear rate of the wheel disc did not seem to be influenced by rail hardness, and even decreased when the rail hardness increased.

Pin-on-disc tests were used to simulate sliding wear. Two wheel materials were used for the disc, wrought wheel of hardness 227HB and cast wheel of hardness 324HB, and the same rail material as in the twin-disc tests for two pins 8mm in diameter. Pin load was 54, 65, 76 and 87 kg. When the softer rail material (235HB) was tested, its wear increased in all experiments using a harder wheel disc, for example by a factor of 5.75 in the experiment with 54 kg load and by a factor of 2 with 87 kg load. When harder rails were tested (278 and 322HB), their wear increased with wheel hardness only in tests with 54 kg load and 65 kg for rail of 322HB, and decreased in all other tests.

The general conclusion was that wear is dependant on both hardness of wheel and rail and that softer components will wear more. In most cases, increasing the hardness of one component will result in a decrease of wear of both components. Pearlite interlamellar spacing was also discussed in the paper and the relationship with wear was established that less wear will occur with smaller interlamellar spacing, and that relationship is more emphasised in sliding wear.

As part of answering a wider research problem of optimization of wheel and rail profiles Zakharov et al. (2006) did laboratory and field tests to see the influence of wheel/rail hardness on wear. Rolling/lateral sliding laboratory experiments of rail-wheel rollers distinguished three hardness levels for influencing wear. For softer material of less than 250HB, total wear does not depend on an increase of one component's hardness. Testing harder rollers 250-450HB showed that if one disc's hardness increased, the total wear of wheel/rail rollers decreased. For a hardness level of more than 450HB, increase in hardness of one component reduced total wear dramatically. The experiments showed decrease of wear of the second component as well.

Field tests were in agreement with the laboratory tests for rail to wheel hardness ratio (HR/HW) from 0.7 to 1.6. This wide range of hardness ratios shows that no magic ratio can be found to provide minimal total wear. In general, wear rate of either component is inversely proportional to its hardness.

Rolling-sliding behaviour of rail steels was studied by Sato et al. (1993) using a twin-disc rolling contact test machine. The wheel disc (driven directly by the motor) was driving the rail disc; both discs constrained to rotate at the same speed by a gear system. Rail material discs were heat treated to give pearlite (280HV, 340HV, and 360HV) and tempered martensite (280HV, 300HV and 360HV)

microstructures. Wheel specimens' material was the same in all tests, with a hardness of 360HV. Tests were conducted under unlubricated and lubricated conditions, with 5% slip, load 750 N (maximum elastic contact stress 525 MPa) for 300000 cycles. The steel tested was Japanese Industrial Standard 60 kg for rail discs and 50 kg for wheel discs.

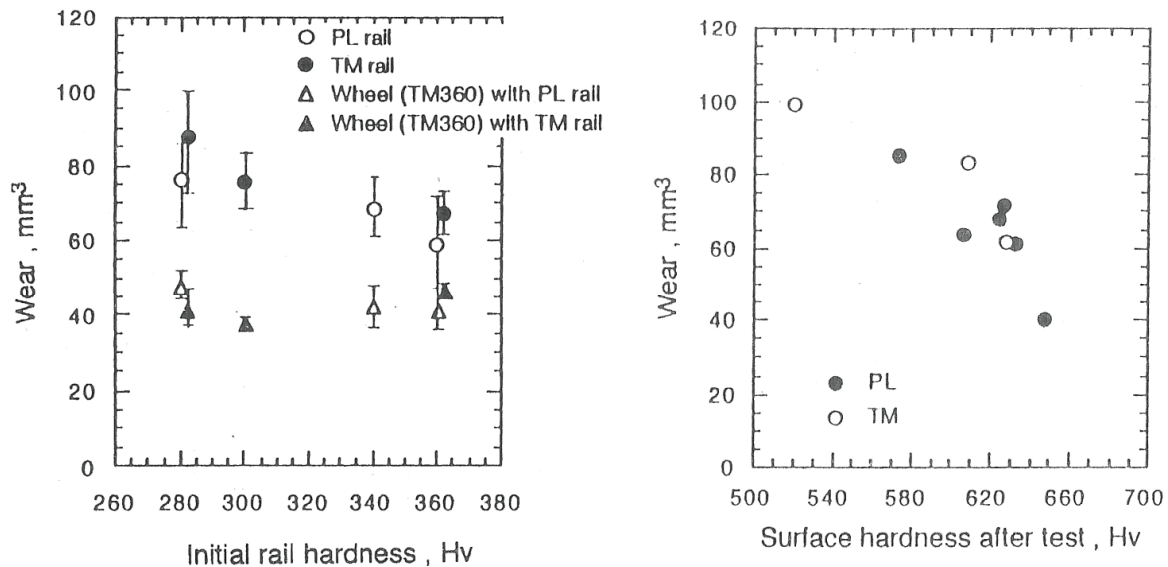


**Figure 15** Left image: Comparison of wear of rail and wheel specimens for different microstructures and different values of rail hardness. Conditions: 750N, 5% slip, unlubricated. Error bars estimated from spread of two or three data points. Right image: Wear of rail specimens for different microstructures and different values of surface hardness after testing. Conditions: 750N, 5% slip, unlubricated. The trends are similar for the two microstructures. (Figures 6 & 7, Sato et al., 1993.)

The wear of rail discs decreased as initial hardness increased for both pearlite and martensite materials in unlubricated tests (see Figure 15).

The influence of increase of surface hardness after testing on wear shows its even higher decrease. Wear of the wheel disc was smaller than that of rail discs. The initial rail hardness and microstructure did not influence wheel wear. In tests where water lubrication followed dry tests, the influence of hardness on volume loss was not very different when materials with different hardness were tested.

British Rail Research (Benson, 1993) conducted a literature survey – *Effect of differential hardness on wheel/rail wear*. Their conclusion was that material microstructure has a more significant role on wear than hardness, so laboratory experiments are needed to investigate the optimum hardness ratio for minimum system wear using materials in the same microstructure group. Across different structure groups, pearlite showed better wear resistance than martensite and bainite, when tested at the same hardness values. When investigating pearlitic steels, up to the level of 380HV, increasing rail hardness resulted in decreases in both rail and wheel wear; above this limit, wheel wear slightly increased. This is the opposite of the general belief that using harder rails wears wheels more. Also, some laboratory experiments showed that optimum rail hardness should be 30% higher than wheel, for minimum system wear, while track data suggest using the same hardness for both. However, increasing rail hardness of pearlitic steels more than 350HV does not have significant influence on rail.

Mädler et al. (2008) performed a series of twin-disc tests on an Amsler-type rig, investigating the behaviour of 6 rail steels (three pearlitic and three bainitic) and 2 wheel steels. (The paper is included as Annex 3.) Disc samples had an external diameter of 46mm (both wheel and rail). Surface pressure was 1250N/mm<sup>2</sup>, and discs rolled with slip of 3% (with the rail disc running at 450 r.p.m., the wheel disc at 436 r.p.m.). Tests were run wet with water lubrication 1 drop every 20s. Three tests were run for each material pair and the results presented are the average of three separate readings. Material loss of wheel and rail samples is presented in Figure 16. When comparing wear rates of wheel steels, using higher-strength B6 material results in lower wear not just for the wheel disc but also for the rail pearlitic steels. Looking at the influence of different rail materials, bainitic steels 1000B and 1100B wear the most and wear of counter wheel disc is slightly higher than when run against the pearlitic rail

steels. Higher strength bainitic rail steel 1400B exhibits lower wear especially when run against R7 wheel. Comparing pearlitic rail steel wear against R7 wheel steel, the best wear resistance is with 350HT grade. There is not a clear trend that harder rail materials wear the wheel more. The general conclusion, when looking at wheel/rail wear as a system, would be to use higher-strength steels for both wheels and rails to get the lowest wear rate of both to maintain profiles longer.

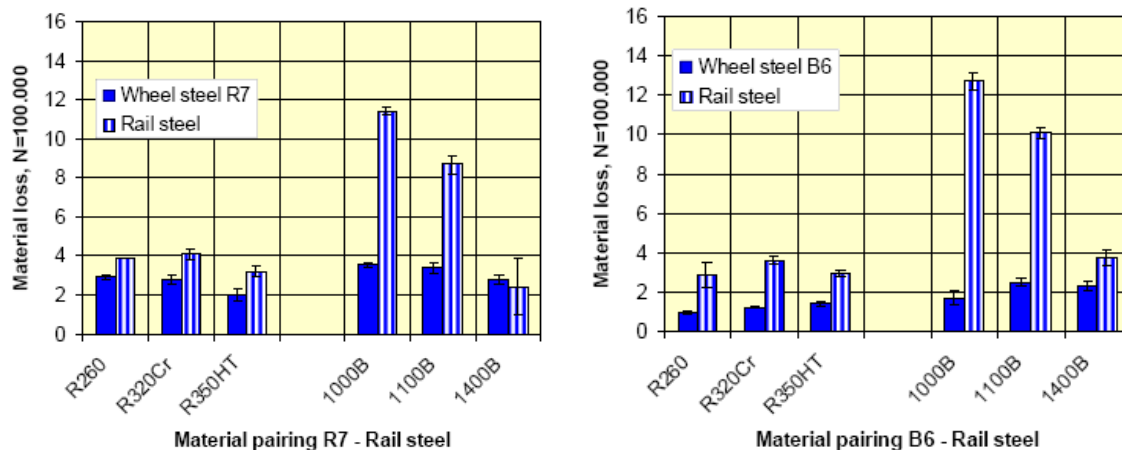


**Figure 16** Material loss on wheel (R7) and (B6) and rail in Amsler test after 100000 roll-overs (Figures 3 and 4, Mädler et al., 2008)

## 4.2 Hardness analysis and discussion

When looking at SUROS test wear data and disc hardness measurements, some conclusions on its correlation can be made, although dependence is not straightforward. Wear rates for both wheel and rail discs for the dry tests are plotted in Figure 17 against both the hardness of the wearing disc and the hardness of opposite, contacting disc.

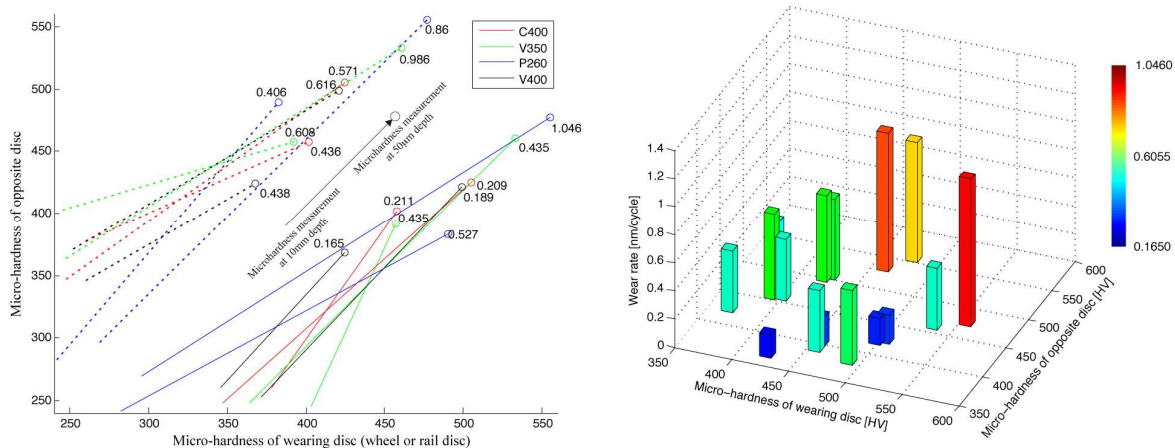


**Figure 17** SUROS test data: Dependence of disc wear on own and opposite disc's hardness for dry tests. Left: Lines are drawn from the micro-hardness measurement at 10mm depth to the (higher) measurement at 50µm depth. Wear rate [nm/cycle] is marked by the circle at the 50µm end. Right: Wear rate for each pair of micro-hardness measurements at 50µm.

Rail disc wear, depending on its own hardness in dry tests (see Figure 18 and Figure 19), shows decrease when rail hardness increases. The same conclusion was made by many researchers (e.g. Pointner, 2008) and it is in agreement with Archard's wear law (Archard, 1953). For softer CORUS 260 material, the difference in the wear rate between numbers of cycles that the test was run is greater than compared to harder materials. For harder materials, wear rate difference is smaller. Wet tests deteriorated softer material more so its wear rate is significantly higher than in dry tests. VA 400 steel showed the lowest wear and it was independent from running number of cycles or environment.

Wheel disc wear (see Figure 18, Figure 19) in dry tests increased when run against harder material VA 350 compared to CORUS 260, but dropped when run against harder steels CORUS 400 and VA 400. However, for 5000 cycles, the lower wheel wear is when run against CORUS 260 rail disc. In wet tests wear rate drops as hardness of rail material increases.

In the system as a whole, using harder CORUS 400 and VA 400 rail steels lowers wear rate and maintains wheel/rail profiles for longer; wear rate did not increase significantly when discs were run from 5000 to 15000 cycles, as observed with tests when CORUS 260 and VA 350 rail materials were used (see Figure 20). Similar behaviour was observed by Madler et al. (2008).

Microhardness measurements of the wheel discs from the twin-disc tests are given in Figure 10.

All discs have shown material hardening characteristics at the surface. Rail material is hardening more when run for more cycles. Softer CORUS 260 steel is hardening more at the surface than harder VA350 and CORUS 400 in dry tests, while the other two materials have similar hardening rates. In wet tests, the CORUS 260 deteriorated a lot and is almost always softer than the other two materials when measured from the surface into the depth of material.

Wheel disc initially had similar hardness values. When microhardness was measured after tests, it hardened the most for 15000 cycles then 10000 (5000 dry + 5000 wet) and the least for 5000 cycles dry. Comparing how much it hardened when run against different materials, in general the harder the rail material becomes, the harder the wheel disc becomes.

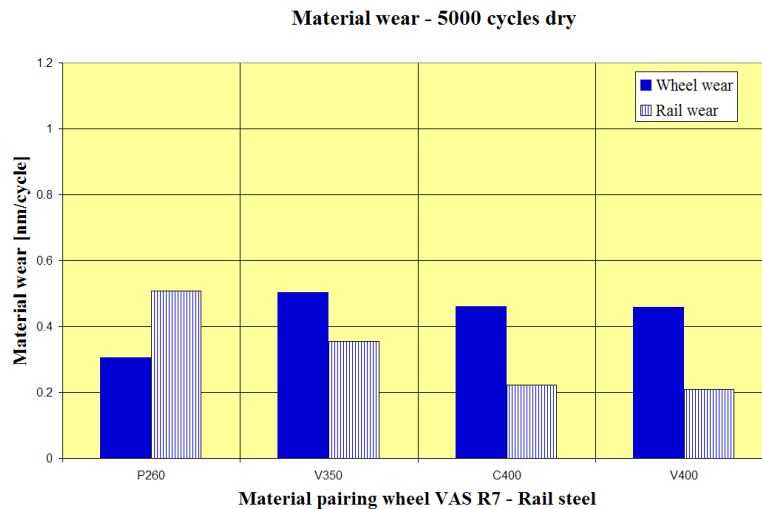


**Figure 18** Material wear on wheel (VAS R7) and rail discs in SUROS test after 5000 cycles dry tests (values are averages of two tests for each material pair).

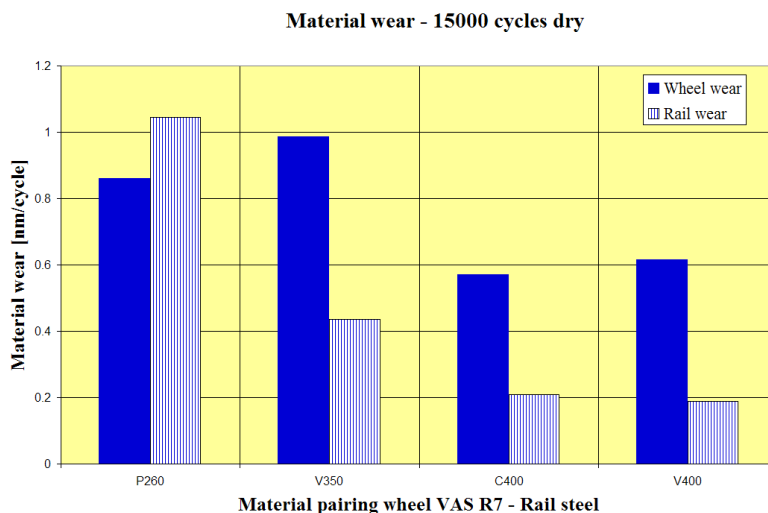


**Figure 19** Material wear on wheel (VAS R7) and rail discs in SUROS test after 15000 cycles dry tests (values are from one test for each material pair).

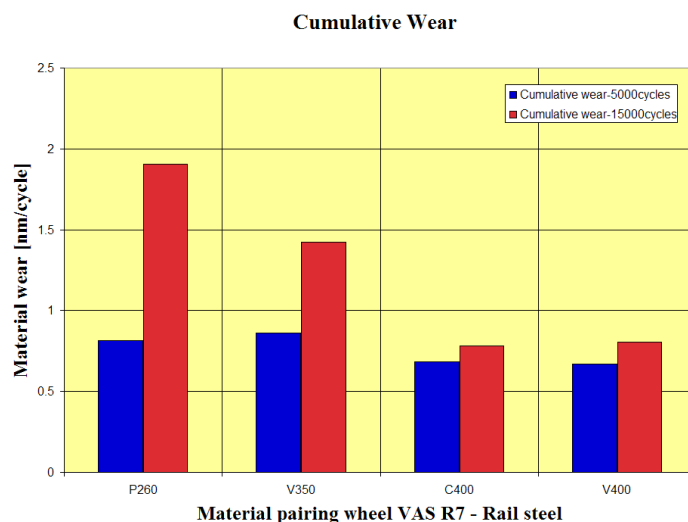


**Figure 20** Cumulative material wear of both wheel and rail discs in SUROS dry tests.

### 4.3 Summary

In general, harder materials wear less. However, material hardness is not the only determining factor of wear performance; microstructure and strain-hardening behaviour are critical factors, and rolling contact fatigue performance is equally important. Regarding the influence of rail hardness on wheel wear, and vice versa, here are some key observations:

**Pointner:** System wear (i.e., considering both wheel and rail) reduces as rail hardness increases – harder rails wear wheels more, but only up to a point, and wear less themselves.

**Markov:** Increasing wheel hardness decreases wheel wear and increases rail wear. In general, the relationship between hardness and wear varies with different test conditions. In most of the experiments that were taken, rail wear rate depends on wheel hardness and it gets higher with harder wheels. When slip is less than 5%, wear rate redistributes according to disc hardness but total wear remains almost the same.

**Singh and Singh:** In all experiments wheel disc wear was higher than rail disc wear. The wear rate of the wheel disc did not seem to be influenced by rail hardness, and even decreased when the rail hardness increased. In most cases, increasing the hardness of one component will result in a

decrease of wear of both components. Regarding sliding wear of pearlitic steel, less wear will occur with smaller interlamellar spacing.

**Zhakarov et al.:** For softer material of less than 250HB, total wear does not depend on an increase of one component's hardness. Testing harder rollers 250-450HB showed that if one disc's hardness increased, the total wear of wheel/rail rollers decreased. For a hardness level of more than 450HB, increase in hardness of one component reduced total wear dramatically. The experiments showed decrease of wear of the second component as well.

**Sato et al.:** There is a clear correlation with rail wear decreasing as rail surface hardness following the test increases, regardless of initial hardness or microstructure. Wheel wear is not sensitive to the rail's initial hardness or microstructure.

**Benson (BRR):** For pearlitic steels up to the level of 380HV, increasing rail hardness decreased both rail and wheel wear; above this limit, wheel wear increased slightly. Some laboratory experiments showed that optimum rail hardness, for minimum system wear, is 30% higher than the wheel hardness, while track data suggest using the same hardness for both. However, increasing rail hardness of pearlitic steels more than 350HV does not have significant influence on rail wear.

**Mädler et al.:** There is not a clear trend that harder rail materials wear the wheel more. The general conclusion, when looking at wheel/rail wear as a system, would be to use higher-strength steels for both wheels and rails to get the lowest wear rate of both to maintain profiles longer.

In conclusion, to reduce system wear, harder steel grades should be used for both wheel and rail.

Additional conclusions from the results of the SUROS tests:

- Rail disc wear decreased when rail steel hardness increased.
- In general, the harder the rail disc material becomes at the surface, the harder the wheel disc material becomes at the surface.
- Wheel disc wear in dry tests was highest when running against VA 350.
- Wheel disc wear in dry tests was higher than the corresponding rail disc wear, except for CORUS 260 which had the highest wear rate.
- In wet tests, wheel disc wear rate drops as rail disc hardness increases.
- In the system as a whole (i.e., considering both wheel and rail discs), using harder CORUS 400 and VA 400 rail steels lowers the total wear rate; also, the wear rate did not increase significantly when discs were run from 5000 to 15000 cycles.

## 5. Wear modelling

---

### 5.1 Development and calibration

#### 5.1.1 Background

The 'dynarat' model (also known as the 'brick' model) was developed initially as a computer simulation of ratcheting wear, based on ratcheting principles outlined by Kapoor (1994), and confirmed experimentally by Tyfour et al. (1996).

The wear simulation was introduced by Kapoor and Franklin (2000), and then developed into a 2D simulation with elements (or 'bricks') which could be given different material properties to better reflect variability of material properties within pearlitic rail steel microstructure (Franklin et al., 2001, 2003). In related work, the effect of surface micro-roughness (even on a polished surface) on ratcheting of near-surface material, i.e., within about 50µm of the surface, shows the importance of considering this effect when modelling wear (Kapoor et al., 2002).

The simulation was first used to look at crack initiation by Fletcher et al. (2003), who used image analysis to identify patterns of failed material elements, and subsequent research has focussed on improving the model's ability to predict life to crack initiation (Franklin and Kapoor, 2007).

An important aspect of the model is its ability to represent rail steel microstructure and, through Rail Research UK, the Universities of Newcastle upon Tyne and Birmingham have collaborated on providing detailed metallurgical data to improve the microstructural model (Franklin and Kapoor, 2007; Garnham et al., 2007). This research is based on careful analysis of twin-disc tests using samples made from British normal grade rail sections, but the goal is to extend the model's capabilities to predict rail life for other grades of rail steel (some preliminary work in this direction is presented by Franklin et al., 2008).

The computer simulation can be used to study wear rates for different combinations of traffic (Fletcher et al., 2008), and in parallel the model is being developed to include thermal effects as a result of frictional heating (Fletcher et al., 2008; Widiyarta et al., 2006).

The 'dynarat' computer simulation has been used in collaboration with industry to calculate wear rates and crack initiation depths for a selection of vehicle cases for sites in the U.K., and also for different rail steel grades – see Appendix 2 of RSSB's Project T355 report "Management and understanding of rolling contact fatigue: Mechanisms of crack initiation" (Burstow, 2008). The simulation has also been adapted for Health & Safety Laboratory (HSL) to study the life of rails with a decarburized surface layer (Fletcher et al., 2006).

#### 5.1.2 The model

The wearing material is modelled as a matrix of rectangular elements representing a cross-section through the material parallel to the direction of traction. This can be used to simulate a rail (for which a fully 3D stress distribution can be calculated and applied in the plane of the simulation) or a twin-disc contact (for which a 2D stress calculation is sufficient). Most of the model's development has been based on twin-disc data, since twin-disc tests allow the load and traction history to be measured. The model calculates elastic stresses for Hertz contacts (elliptic pressure and traction distributions); although the simulation models plastic shear strain accumulation, the elastic stress state is considered to be a good approximation for contact loads close to the shakedown limit.

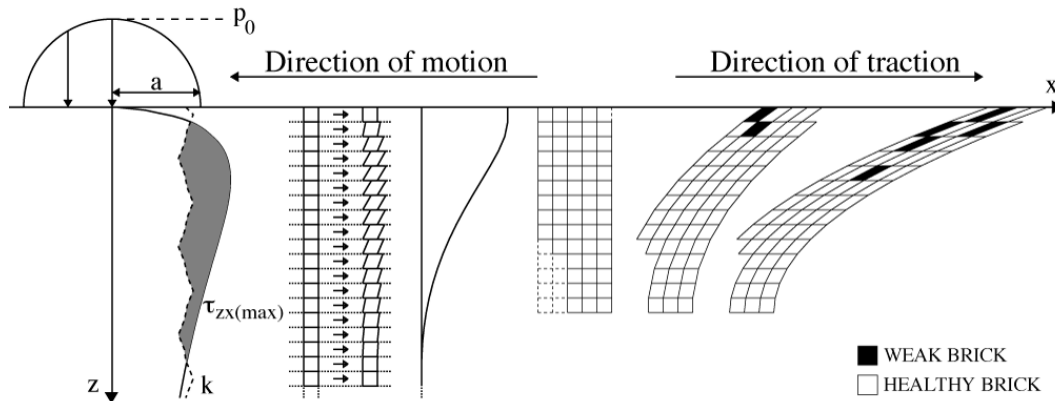


**Figure 21** Left: A single increment of plastic shear strain. Right: As the shear strain accumulates, material fails and elements (or ‘bricks’) are marked as ‘weak’.

The plastic shear strain at depth  $z$  is determined by the maximum orthogonal shear stress,  $\tau_{zx(max)}$ , occurring at depth  $z$ . Where, as in the grey-shaded region of Figure 21, this exceeds the yield stress in shear,  $k$ , there is an increment of plastic shear strain proportional to the difference. In this case, the traction coefficient is zero, so there is no shear stress at the surface, but usually (and certainly in twin-disc tests which simulate a driving wheel) there will be traction opposite to the direction of motion; and the shear yield stress varies with depth, reflecting the variation in shear yield stress between different elements. The whole matrix of elements deforms each cycle, and the deformation increases over thousands of load cycles. Eventually the ductility of the material is exhausted and material starts to fail; failed elements are marked here as ‘weak’.

Each element in the matrix is given material properties, in particular the initial shear yield stress,  $k_0$ , and the critical plastic shear strain,  $\gamma_c$ , at which the element will fail. The properties are assigned in a pattern representing the microstructure. The hexagonal pattern in Figure 22 and Figure 23 is easy to configure in terms of grain size and grain boundary width, and can be rotated. The properties of the ‘pearlite’ (technically a lamellar structure of cementite and ferrite) and ferrite can also be configured.

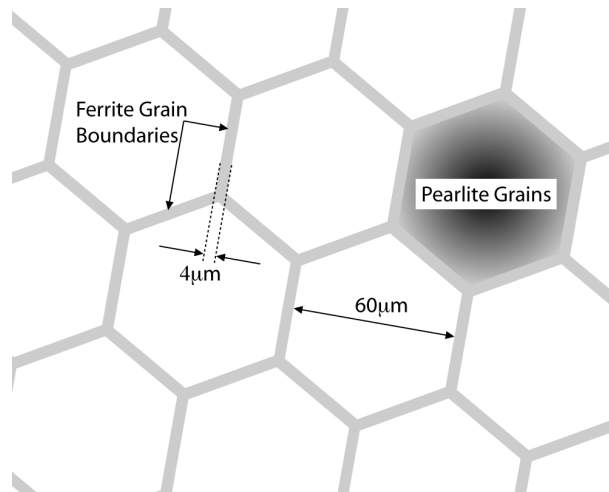


**Figure 22** Pearlitic steel microstructure represented as hexagonal grains of ‘pearlite’ surrounded by pro-eutectoid ferrite at the prior-austenite grain boundaries.

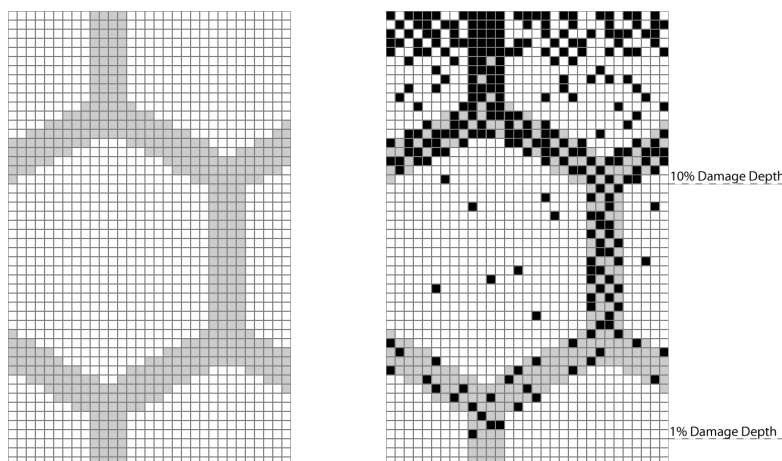


**Figure 23** Left: Matrix of elements, with ferrite elements coloured in dark grey, and pearlite elements coloured in light grey. Right: Since the pearlite is harder than the ferrite, failure occurs sooner in the ferrite (failed elements coloured in black).

**Table 5.** Measured nano-hardness,  $h$ ; ratio of final (asymptotic) hardness to initial hardness,  $\beta$ ; critical plastic shear strain at which failure occurs,  $\gamma_c$ .

Material	$h$ (kgf/mm <sup>2</sup> )	$\beta$	$\gamma_c$
Ferrite	250	1.48	11
Pearlite	370	1.55	11

As plastic shear strain accumulates, the material hardens. (A detailed analysis and model of this is given by Kapoor et al., 2004.) The material properties of ‘pearlite’ and ferrite, determined for normal grade rail steel, are given in Table 5. Shear yield stress is proportional to the measured nano-hardness (see Garnham et al., 2007, and Franklin and Kapoor, 2007):

$$k = 0.8 \times 10^6 h$$

where the units of  $k$  are Pa and the units of  $h$  are kgf/mm<sup>2</sup>.

### 5.1.3 Model calibration

Prior to InnoTrack, dynarat wear model calibration and development has focused on British normal grade rail steel which has a significant proportion of pro-eutectoid ferrite at prior-austenite grain boundaries, and which therefore is best modelled as a two-material (ferrite / ‘pearlite’) microstructure. However, the harder 260 grade and the 350 and 400 premium grades do not have such a high proportion of pro-eutectoid ferrite and in this work a single material (‘pearlite’) microstructure is used, and the properties of the ‘pearlite’ calibrated using the recorded traction data, and the shear strain and microhardness measurements presented in Section 3.

The aim is to partly calibrate the wear model while leaving the opportunity also to validate it.

- For all four rail steel grades tested, the principal aim is to calibrate the initial hardness and strain-hardening behaviour.
- For the 260 grade only, the aim is also to calibrate the wear rate against twin-disc results.
- Wear rate predictions will be made for the premium grade rail steels, and compared against measured twin-disc results.

The complete set of microhardness measurements is tabulated in Annex 1. One unusual observation, which may be nothing more than measurement error or an indication of hardness variation in the original railhead, is that hardness measurements are slightly lower (93-96%) at 2-5mm compared with the measurements at 10mm which are used as a baseline / core hardness reference. However, if this is a real effect, it suggests that the materials soften slightly for very small strains. (Softening of some steels at small strains has been noted by other researchers; see, e.g., Sankaran et al., 2003.)

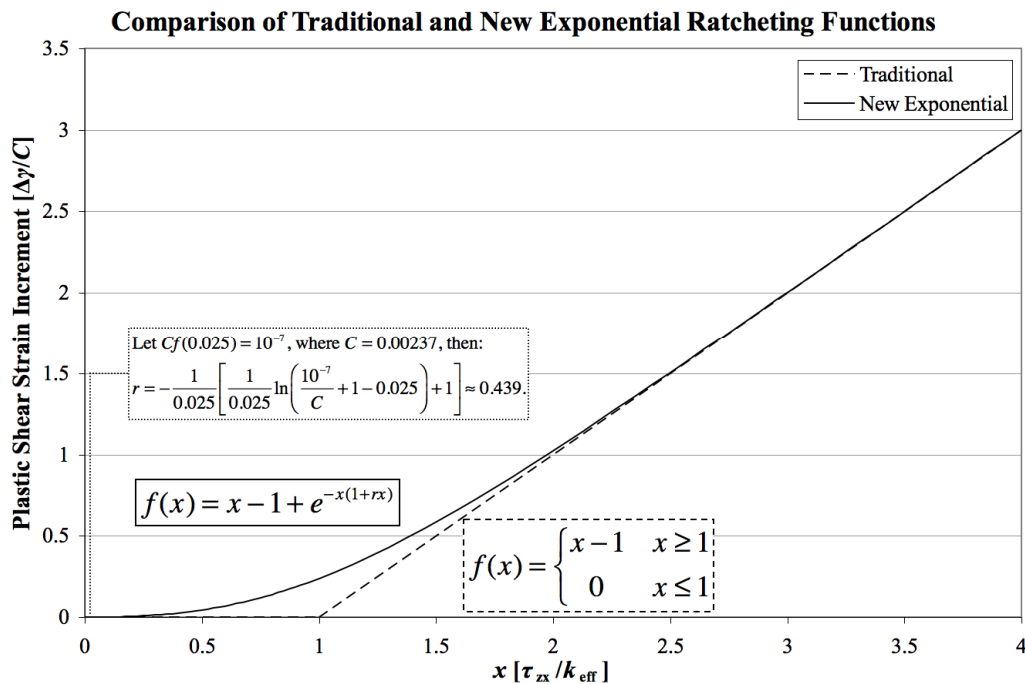


**Figure 24** Comparison of traditional and new ratcheting equations.

Another observation is that the micro-hardness readings would need to be scaled by a factor of about 0.4. A similar factor was needed when calibrating against nano-hardness (see Garnham et al., 2007), justified because hardness readings scale with indent size.

However, rather than introduce an arbitrary scale factor, the alternative approach followed here is to modify the ratcheting equation. The traditional equation has a sharp cut-off at the shear yield stress, and therefore the computer simulations predict zero strain accumulation when the applied orthogonal shear stress drops below this. The two equations are shown in Figure 24. The choice of equation is arbitrary, but the new ratcheting equation meets the following requirements:

- it is asymptotically equivalent to the traditional equation (and tends to the asymptote quickly) as the shear stress increases;
- it drops rapidly to zero (but remains finite) as the shear stress decreases;
- the shear strain increment is still significant when the ratio of shear stress to shear yield stress is 0.4 (i.e., rather than scale the hardness by 0.4, ensure that strain will accumulate when the shear stress is 0.4 times the shear yield stress); and
- it fixes the shear strain increment to  $10^{-7}$  (so that the accumulated shear strain is  $10^{-3}$  after 10000 cycles) when the ratio of shear stress to shear yield stress is 0.025 (i.e., at a depth of about 5mm).

The last bullet point makes it easier to reproduce the observed softening behaviour if an appropriate strain-hardening equation is chosen. (Of course, this has negligible effect on the wear rate.) The modified Voce equation used traditionally does not permit softening, but the following equation has a reasonable fit to the data:

$$H(\gamma) = H_0 \left[ a \ln(1 + \gamma^b) + c + (1 - c)e^{-x/d} \right]$$

**Table 6.** Strain-hardening parameters for the different pearlitic rail steels tested.

Rail Steel	Core Hardness	a	b	c	d
Corus 260	296.0	0.260177580	1.292291910	0.96	0.0001
Corus 400	347.0	0.224138139	1.399843934	0.95	0.0001
VA 350	364.0	0.396849778	0.823357015	0.95	0.0001
VA 400	371.5	0.206666114	1.310212528	0.93	0.0001

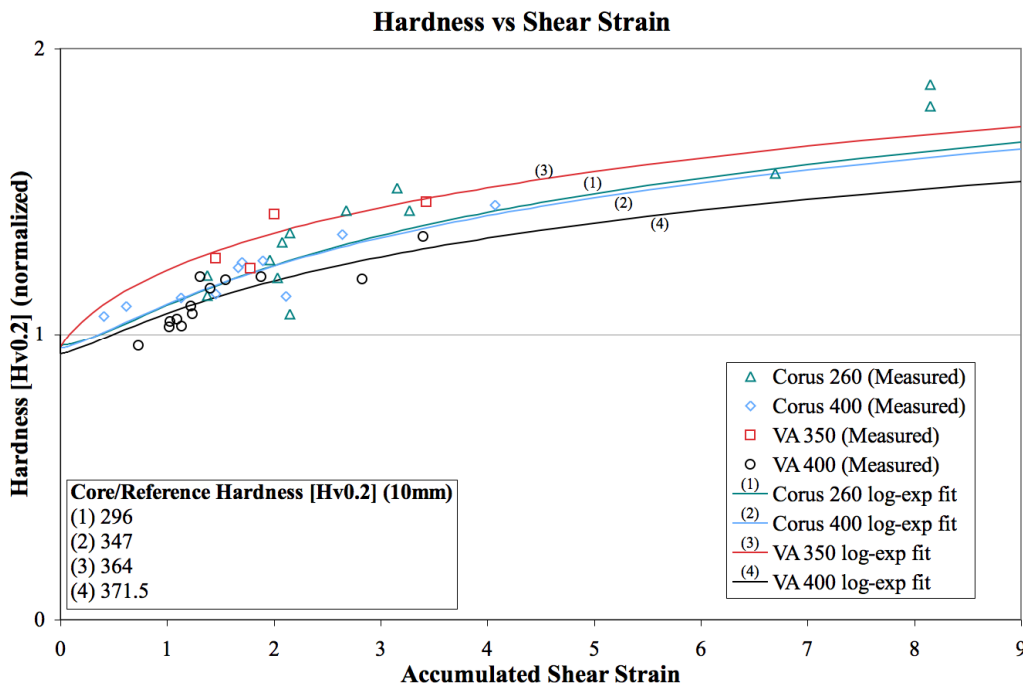


**Figure 25** Strain-hardening curves and measured data from twin-disc tests.

The five constants in the equation are tabulated for the four grades of rail steel in Table 6 and shown in Figure 25. (This is an early analysis; there is clearly room for an improved fit.)

To complete the calibration of the model against the microhardness data, the equation used to amplify stresses near the surface (used to model the effect of surface micro-roughness of the opposite contacting surface – see Franklin and Kapoor, 2007) was changed to:

$$A \left( \frac{z}{d} - 1 \right)^2 - 1$$

where A=3.5 and d=200µm.

Wear simulations were performed for the 260 grade using the new ratcheting and strain-hardening equations. An area of 0.5mm (width) × 10mm (depth), with element size 1µm×1µm, was modelled, with one simulation corresponding to each twin-disc test. (In addition, simulations with an area of 0.05mm × 0.05mm, with element size 0.1µm×0.1µm, were performed to confirm that element size does not affect wear rate significantly.) The contact data was based on the measured history of traction coefficient for the 5000 cycles dry and 15000 cycles dry tests. Material properties (hardness and critical shear strain) were allowed to vary by 5% between elements in the mesh.

Wear rate can be calibrated by adjusting the critical shear strain; increasing this will reduce the wear rate. Unfortunately, this method is not sufficient to get a good match to experimental data, so a new wear methodology has been developed for the computer simulation. Instead of defining the critical shear yield strain ( $\gamma_c$ ) as a threshold value below which material is healthy and above which material is weak, i.e., as a very black-and-white scenario (see Figures 21 and 23), it is defined as a reference value and a ‘weakness’ value between 0 and 1 is calculated for each material element:

$$p \propto \frac{\gamma / \gamma_c}{1 + \gamma / \gamma_c}$$

This weakness value is then used to calculate the instantaneous probability of wear. A value of critical shear strain,  $\gamma_c=29$ , was chosen so that predicted wear rate of the Corus 260 matched test measurements well. The same value of critical shear strain was then used when simulating other rail steel grades; wear rates are given in Table 7. The complete set of figures showing the predicted micro-hardness with depth, and the predicted accumulated plastic shear strain with depth, are given in Annex 2.

**Table 7.** Predicted wear rates [nm/cycle] from simulations of the twin-disc tests, and measured wear rates (from Table 3).

Predicted	5000	10000	15000	Measured	5000	10000	15000
P260	0.314	0.550	0.972	P260	0.527	4.833	1.046
C400	0.271	0.409	0.809	C400	0.211	1.040	0.209
V350	0.169	0.344	0.629	V350	0.435	0.377	0.435
V400	0.226	0.426	0.898	V400	0.165	0.467	0.189

The wear rate predictions for the premium grade rail steels match measured values (approximately) for the 5000 cycles dry tests, but over-predict the wear rate for the 15000 cycles dry tests by a factor of 2-3. (The dry-wet test predictions do not match, but are not expected to, since the ratcheting wear model does not account for major surface deterioration caused by significant surface cracking.)

## 5.2 Different vehicle characteristics

The wear model is sensitive to vehicle characteristics through their effect on the wheel-rail contact patch, in particular contact patch size and shape, normal load and traction coefficient. This study makes the following assumptions:

1. The contact patch shape is elliptical and the pressure distribution is Hertzian. Longitudinal semi-contact width ( $a_L$ ) and transverse semi-contact width ( $a_T$ ) are calculated from the normal load using the following simplified relation derived by Chalmers for wheel-rail contact on top of the rail head (i.e., appropriate for straight track, not curves):

$$a_L = 1.57 \times 10^{-4} \times \sqrt[3]{F}$$

$$a_T = 1.19 \times 10^{-4} \times \sqrt[3]{F}$$

where  $F$  is the normal load. The peak pressure is given as usual by:

$$p_0 = \frac{3}{2} \frac{F}{\pi a_L a_T}$$

2. The friction coefficient is constant and equal to 0.45. Effects of lubrication, rain water and track contaminants are not studied here. (The dynarat wear model used here is the 260 grade model calibrated in Section 5.1 for dry contact.)
3. The vehicle condition selected as a 'standard' case for this study is a normal load of 100kN (approximating a 20-tonne axle load) and traction coefficient 0.3. Only longitudinal traction is considered.

For partial slip conditions (i.e., when the traction coefficient is less than the limiting friction coefficient) the wheel-rail contact region can be divided into 'stick' regions and 'slip' regions. In general, these regions move dynamically, making it difficult to model the contact patch. A new static model of partial slip has been developed for the dynarat wear model.

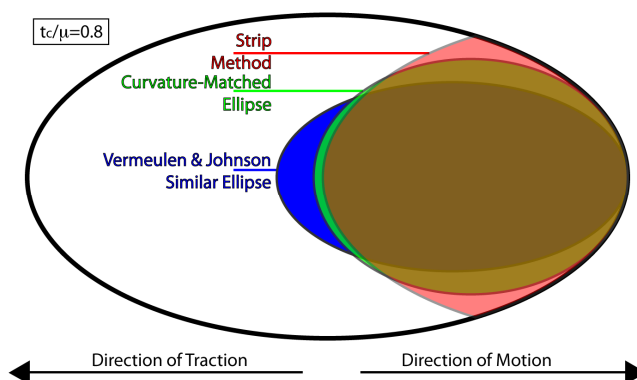


**Figure 26** Three models for the adhesive ('stick') zone in a partially slipping contact.

The two standard approaches to modelling the adhesive ('stick') zone are the 'similar ellipse' method developed by Vermeulen and Johnson (1964) and the strip method developed by Haines and Ollerton (1963). The 'strip method' is a more accurate representation of the adhesive zone as observed in experiments, whereas the similar ellipse method is computationally simpler. The new model also has an elliptical adhesive zone, thus retaining the computational simplicity of the similar ellipse method, but chooses an ellipse which matches the curvature of the contact patch exactly and which thus provides a closer match to the strip method's 'lemon'-shaped adhesive zone.

The effect of traction coefficient and transverse offset of the contact (see Figure 27) are studied for normal load 100kN and for a range of longitudinal traction coefficients. Wear rate, averaged over 100000 cycles, is shown in Figure 28. Wear rate is maximum at the centreline of the contact, dropping to zero at the edges of the contact. The average wear rate across the full width of the contact is about 75% of the wear rate at the centreline.

Traction coefficient has a significant effect on the wear rate. For unpowered coaches there should be no traction on straight track (except when braking, on approach to a station, for example). For distributed traction systems the traction coefficient may often be about 0.1, corresponding to the lowest of the three curves in Figure 28, i.e., an average wear rate of about 0.75nm/cycle. For locomotives the traction coefficient may be 0.3 or even higher, i.e., an average wear rate of 1.5nm/cycle or more.

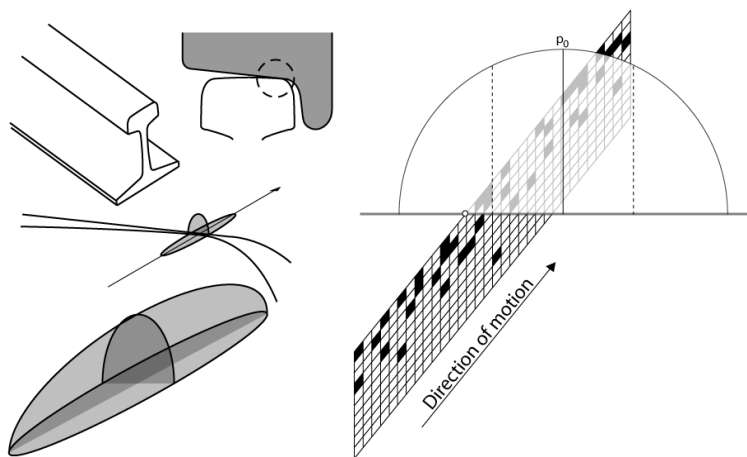


**Figure 27** The wheel-rail contact patch is an ellipse, and the pressure distribution is also elliptical. Usually the dynarat wear simulation models a plane through the centreline of the contact, but it is also possible to offset the model's plane from the centreline.

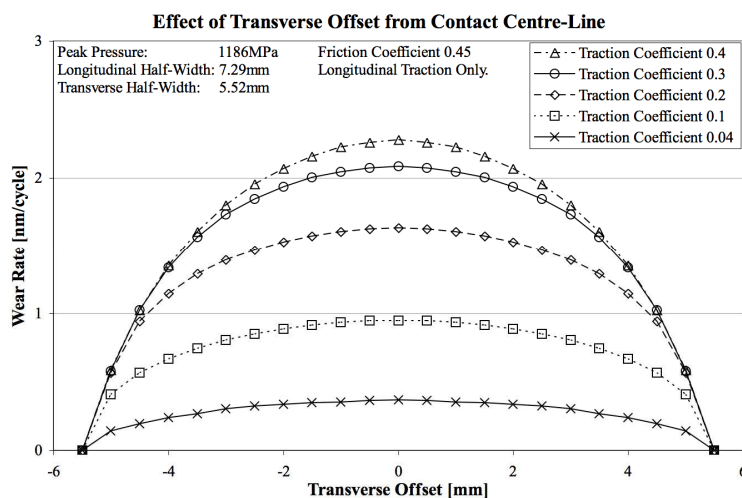


**Figure 28** Predicted wear rates, averaged over 100000 cycles, for a range of (longitudinal) traction coefficients (with friction coefficient 0.45) and normal load 100kN. The transverse half-width is 5.52mm, and wear rates are evaluated in 0.5mm intervals from the centreline to the edge of the contact.

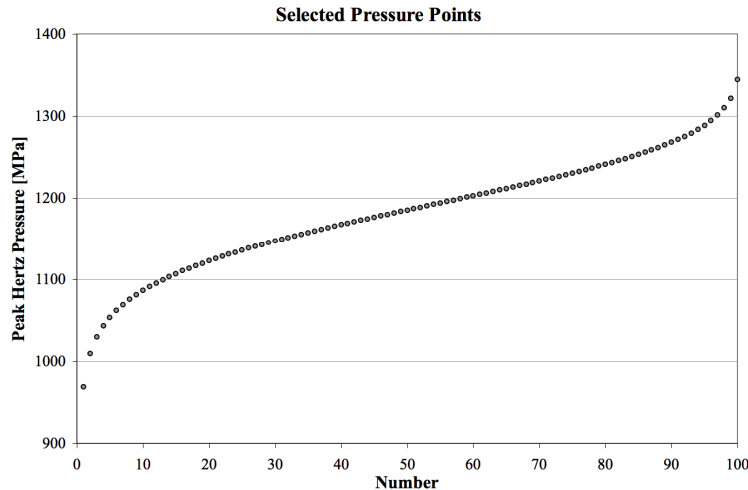


**Figure 29** 100 pressures selected to represent a normal (i.e., Gaussian) variation of contact loads (mean: 100kN; standard deviation 25kN).

To study the effect of contact pressure on the wear rate, and also to study the effect of contact force variation caused by out-of-round wheels, a distribution of pressures representing normal variation of contact force was selected (see Figure 29). A wear simulation was performed for each pressure, and Figure 30 shows the wear rate averaged (a) over the whole 100000 cycles (b) over the first 10000 cycles, and (c) over the last 10000 cycles. The last is a prediction of the asymptotic 'steady state' wear rate. For all three averaging periods, there is a clear linear trend, and the equations of the linear fits are given in Figure 30. Together, Figures 28 and 30 suggest the following wear equation:

$$w = 0.2 \frac{t_c}{\mu} \left( 3 - \frac{t_c}{\mu} \right)^2 (2.3p - 0.68)$$

where  $p$  is peak pressure in GPa, and  $w$  is average wear rate in nm/cycle; friction coefficient  $\mu=0.45$ . To calculate profile area loss, the wear rate should be multiplied by the width of the contact.

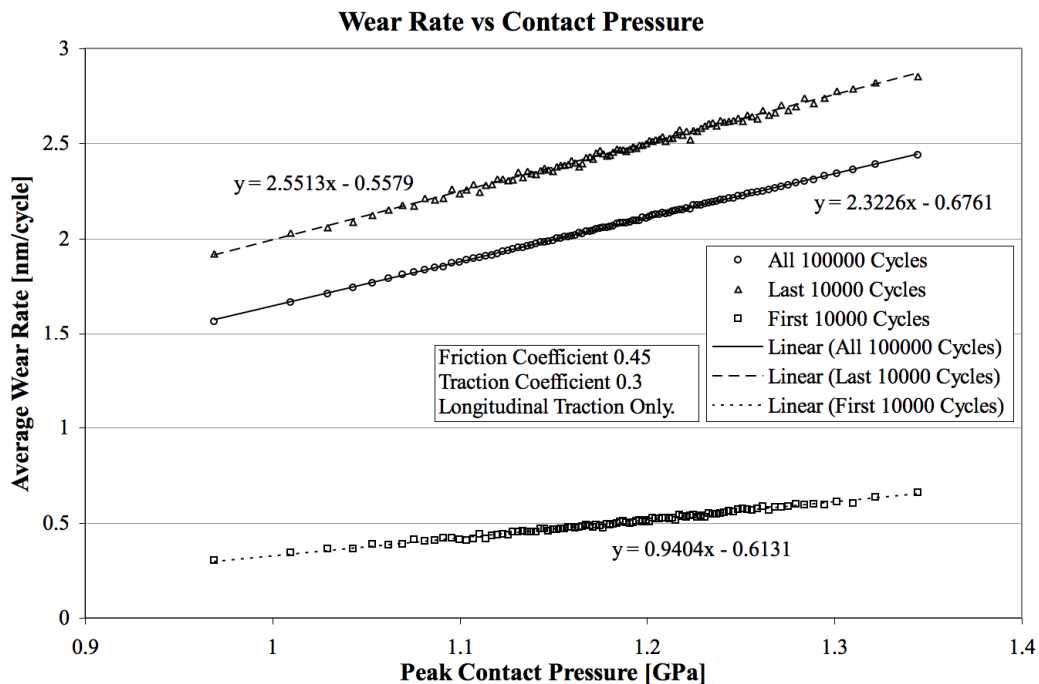


**Figure 30** Wear rates from simulations over 100000 cycles showing the effect of pressure.

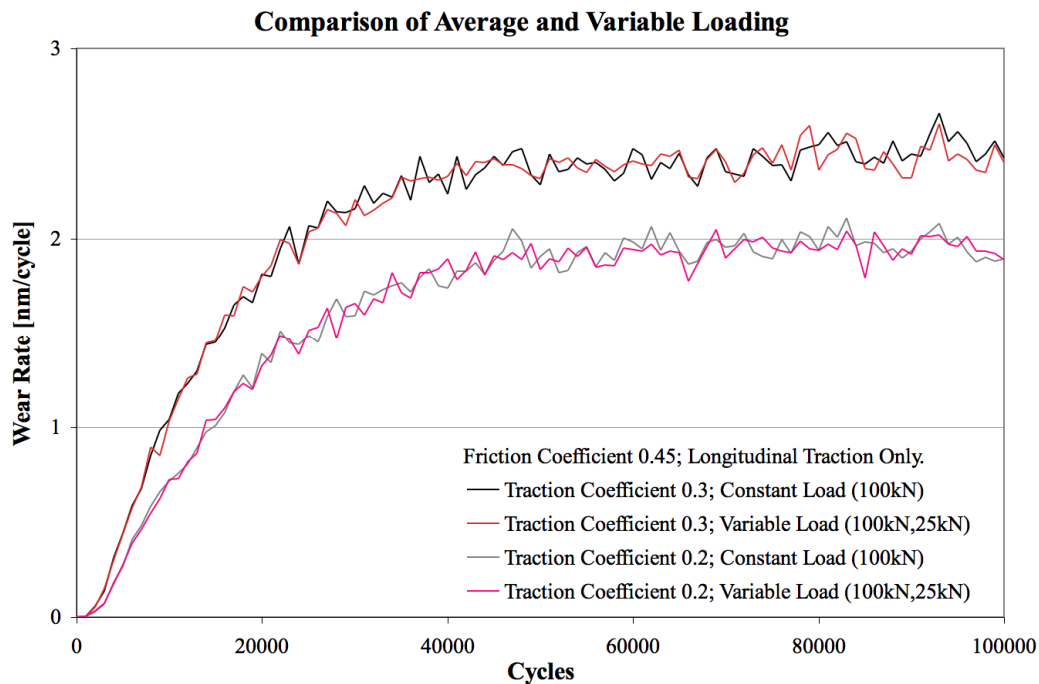


**Figure 31** Effect of contact pressure variation (between wheel passes) caused by out-of-roundness. Simulations with (longitudinal) traction coefficients 0.2 and 0.3, compared with respective constant pressure equivalent cases.

In Figure 30 the contact pressure was the same for each wheel pass during the simulation. To study the effect of out-of-round wheels on the wear rate, simulations were performed in which each wheel pass had a different pressure chosen at random from the selection in Figure 29. This was done for two traction coefficients, 0.2 and 0.3, and the results are compared in Figure 31 with simulations in which the contact pressure was constant (the average pressure) for each wheel pass. The pressure variation does not have a significant effect on the wear rate in either case, suggesting that out-of-round wheels do not need to be considered in wear rate calculations.

### 5.3 Summary

Four pearlitic rail steels (CORUS 260, CORUS 400, VA 350 and VA 400) were tested against VAS R7 wheel steel. Three twin-disc tests were performed for each rail steel: 5000 cycles dry; 5000 cycles dry followed by 5000 cycles wet (i.e., water-lubricated); and 15000 cycles dry. The mixed (dry-wet) tests caused severe rolling contact fatigue, affecting hardness readings and wear rates, but the dry tests have provided an excellent resource for wear model development and calibration.

The aim was to partly calibrate the wear model while leaving the opportunity also to validate it. Therefore, material hardness models were developed and calibrated for all four rail steels, but the wear model itself was calibrated only against CORUS 260, so that wear predictions for the premium grade rail steels could be used for validation.

Test specimens have been sectioned analysed by taking microhardness measurements and shear strain estimates. Microhardness measurements have suggested a possible softening effect at very small strains, and a new strain-hardening equation is used to fit to the strain-hardness data for each of the four steels.

In addition to a new hardening equation, wear model calibration has led to the introduction of:

- a new ratcheting equation, asymptotically equivalent to the traditional ratcheting equation but which permits shear strain accumulation when the applied stress is less than the shear yield stress;

- a new 'greyscale' approach to ductility exhaustion and failure in which material elements are given a number between 0 and 1 representing 'weakness' rather than the traditional 'black-and-white' approach in which material elements are treated as either 'healthy' or 'weak'; and
- a new quadratic equation for modelling the effect of roughness of the opposite surface (e.g., the effect of wheel roughness on rail stresses).

The wear rate predictions for the premium grade rail steels match measured values (approximately) for the 5000 cycles dry tests, but over-predict the wear rate for the 15000 cycles dry tests by a factor of 2-3. (The dry-wet test predictions do not match, but are not expected to, since the ratcheting wear model does not account for major surface deterioration caused by significant surface cracking.)

The wear model, calibrated for CORUS 260 and dry contact, was used to study the effect on rail wear of vehicle characteristics through their effect on the wheel-rail contact. The patch was assumed to be elliptical and the pressure distribution to be Hertzian; in addition, the contact was assumed to be on the top the rail, suitable for straight track, not curves, and the traction to be longitudinal only. A new static partial slip model was used to study the effect of traction.

Traction coefficient has a significant effect on the wear rate. For distributed traction systems the traction coefficient may often be about 0.1, i.e., an average wear rate of about 0.75nm/cycle. For locomotives the traction coefficient may be 0.3 or even higher, i.e., an average wear rate of 1.5nm/cycle or more.

There was a very clear linear trend of wear rate against peak contact pressure (for the range of pressures studied).

The effect of out-of-round wheels was studied by varying the normal load with each passing wheel, and comparing this with the constant average-load case; no significant difference was observed.

## 6. Crack modelling

---

### 6.1 OOR and contact stress-driven crack propagation

The crack propagation model developed by Fletcher et al. (see D4.3.1, Annex IX) can be used to study the effect of out-of-round wheels on crack propagation. The model has been developed to allow cyclic variation of contact pressure with contact location relative to the crack mouth. This is suitable for studying the effect of short-wavelength high spatial frequency pressure fluctuations; longer-wavelength fluctuations (i.e., much longer than the crack size) can be studied effectively using the original model with different (constant) contact pressures.

The wheel-rail contact pressure is varied according to contact location relative to the crack mouth using the equation:

$$p_0 = p_a + a \sin(kx + \phi)$$

In this study, the mean pressure ( $p_a$ ) is fixed at 1750MPa for out-of-round (OOR) and non-OOR ('static') simulations, and the amplitude of pressure variation ( $a$ ) is fixed at 200MPa for OOR simulations (see Figure 32). The wheel-rail contact is elliptical (3.9mm lateral half width, and 5.9mm longitudinal half width) with a Hertz pressure distribution; the friction coefficient (on the surface and in the crack face) is 0.15, representing water lubricated contact. The effects of frequency ( $k$ ) and phase ( $\phi$ ) are studied here.

For a fixed semi-circular surface-breaking crack size of radius 6.5mm at 30° below the surface, the effect of contact pressure variation on the Mode I and II stress intensity factors ( $K_I$  and  $K_{II}$ ) is shown in Figure 33, along with calculations for static cases representing the mean (1750MPa) and limits (1550MPa and 1950MPa). The stress intensity factors can be seen to oscillate between these two limits.

Crack growth rate depends on the stress intensity factor range, i.e., the difference between the maximum and minimum stress intensity factors (or simply maximum  $K_I$  value since this varies from zero upwards). These are plotted against crack radius in Figure 34. In Figure 34(b) it is clear that pressure variation increases the stress intensity factor range, especially for longer cracks, so that the higher pressure determines the trend, i.e. the variable pressure case approaches the upper limit. This is apparent also in Figure 35 which shows crack growth rate against crack radius, where again the growth rate with variable pressure tends to the prediction for the higher (static) pressure.

In Figure 36, the effect of varying the phase angle is shown. Variable pressure with 1750MPa, for a selection of phase angles, is compared against static pressure cases for 1550MPa and 1950MPa. In all cases, the predicted crack growth rate for the variable 1750MPa follows close to the static 1950MPa curve. Phase angle has a slight but not significant effect on crack growth rate – as would be expected for the frequency examined, at which multiple load peaks take place during the passage of the wheel over the crack.

The frequency was fixed with  $k=4000\text{m}^{-1}$  in the above analysis. The effect of varying frequency is shown in Figure 37. For values of  $k$  higher than  $3000\text{m}^{-1}$ , the effect of frequency is not significant, and the predicted crack growth rate lies close to the prediction for static pressure 1950MPa. For lower frequencies, the predicted crack growth rate varies substantially between the predictions for 1550MPa and 1950MPa, and phase angle has a more significant effect.

These results indicate that:

- for pressure variations with a wavelength less than about 2mm, the maximum pressure should be used to calculate crack growth rate; and
- for wavelengths greater than about 20mm, there is no advantage to modelling pressure variation within a single load pass, and that modelling successive wheel passes with different static pressures would be sufficient.
- out-of-round wheels with roughness features between these two wavelengths would accelerate crack propagation, but would require more detailed modelling.

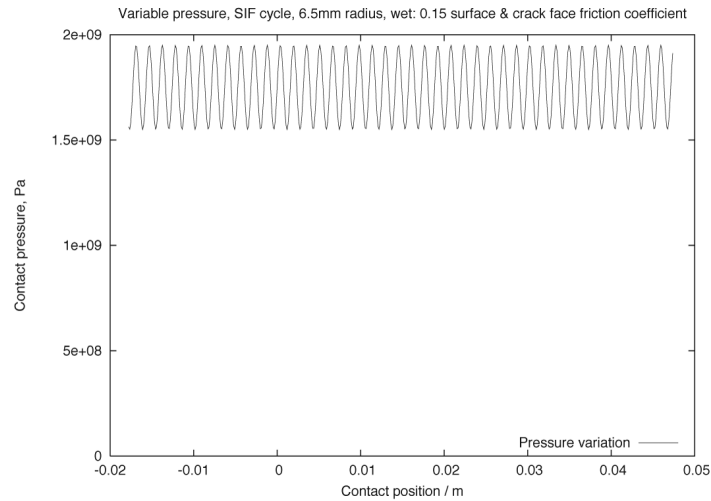
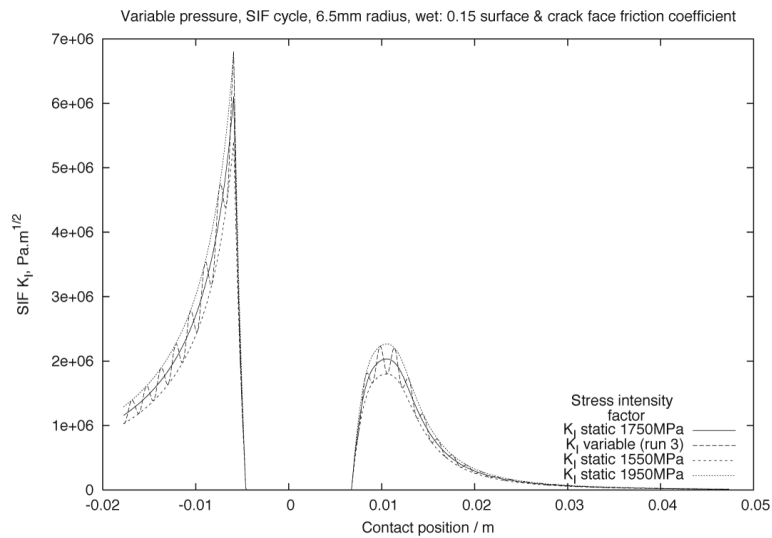
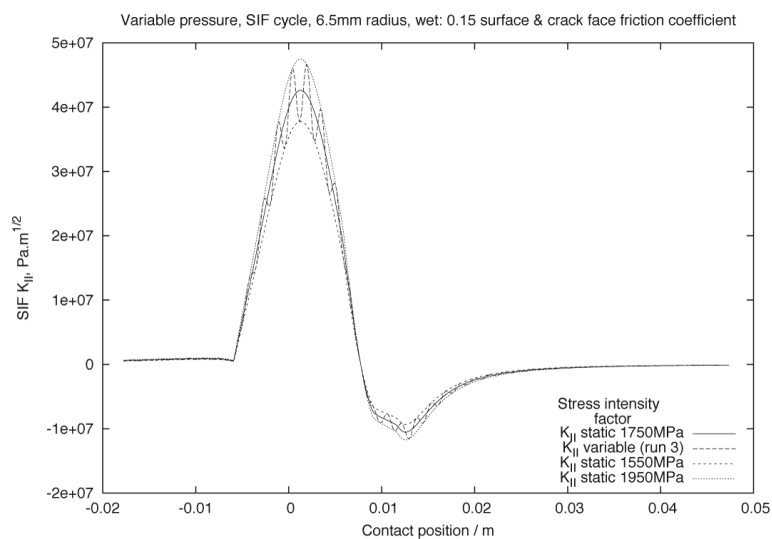


**Figure 32** Input contact pressure for variable pressure crack growth rate calculations. The crack mouth is at the origin.

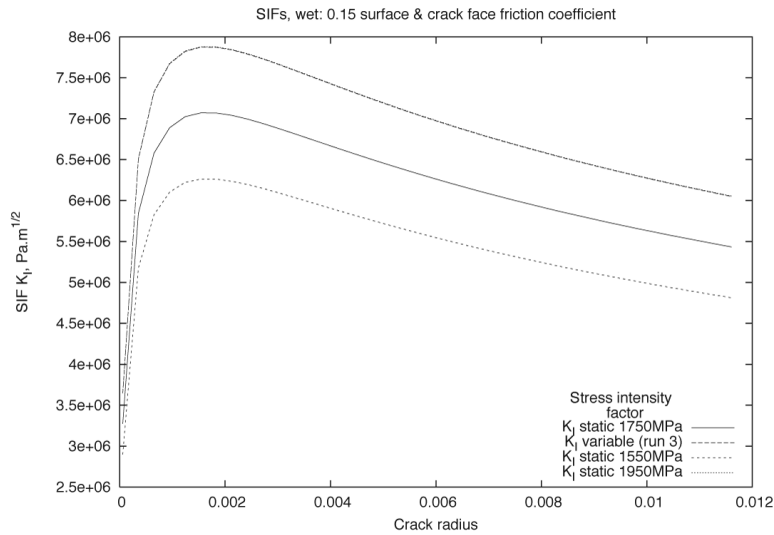


(a)

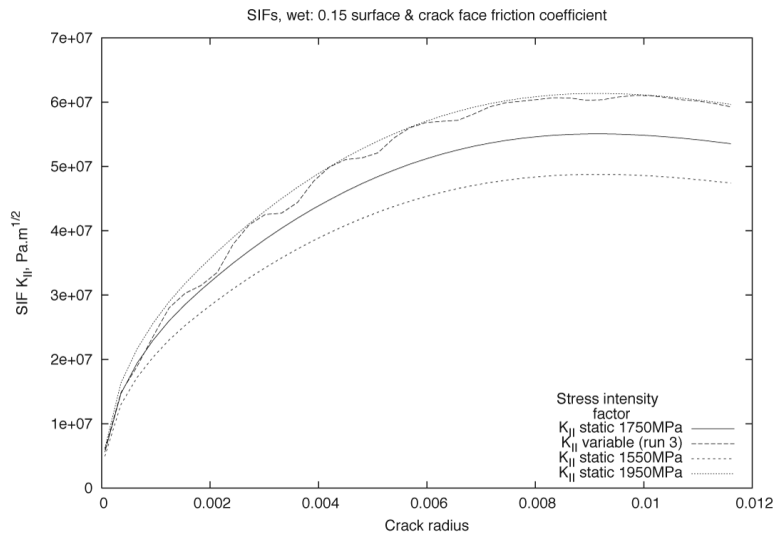


(b)

**Figure 33** Stress intensity factors for contact centre relative to crack mouth, in crack opening Modes I and II respectively. Crack radius 6.5mm.



(a) Mode I data. Curves for 1950MPa and the variable pressure run are almost indistinguishable.



(b) Mode II data.

**Figure 34** Stress intensity factor range vs crack radius, in crack opening Modes I and II respectively. The variable pressure case (labelled Run 3) took place at 4000m<sup>-1</sup>, with a phase angle of zero.

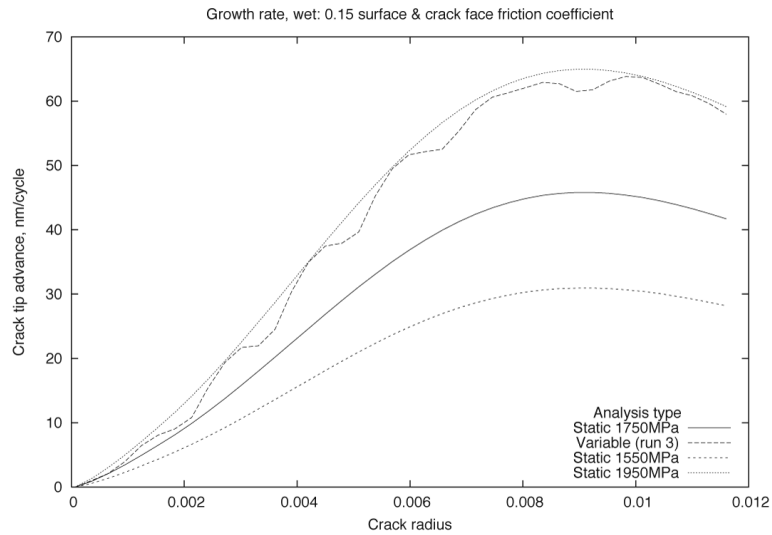


**Figure 35** Crack growth rate vs crack radius, showing that crack growth will be faster for the variable contact pressure. The variable pressure case (labelled Run 3) took place at 4000m-1, with a phase angle of zero.

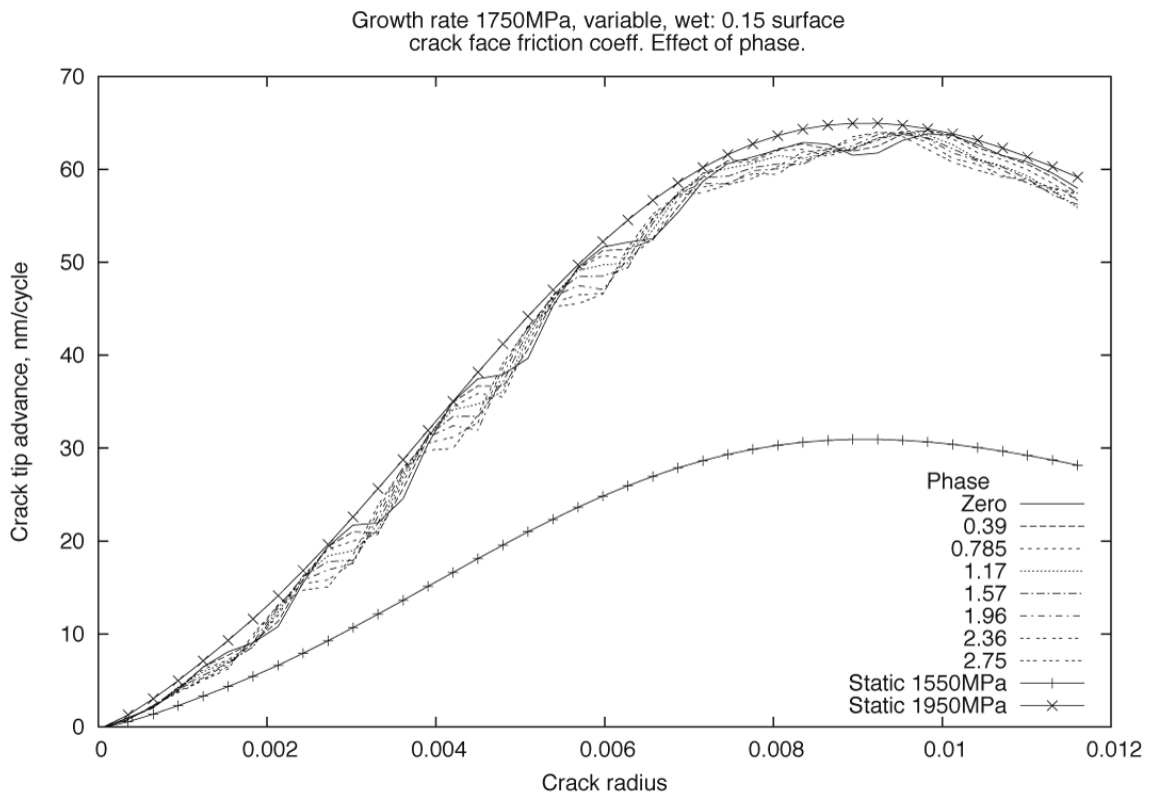


**Figure 36** Effect of phase on crack growth rate. Phase angle is varied for variable 1750MPa pressure, and compared with static 1550MPa and 1950MPa pressures.

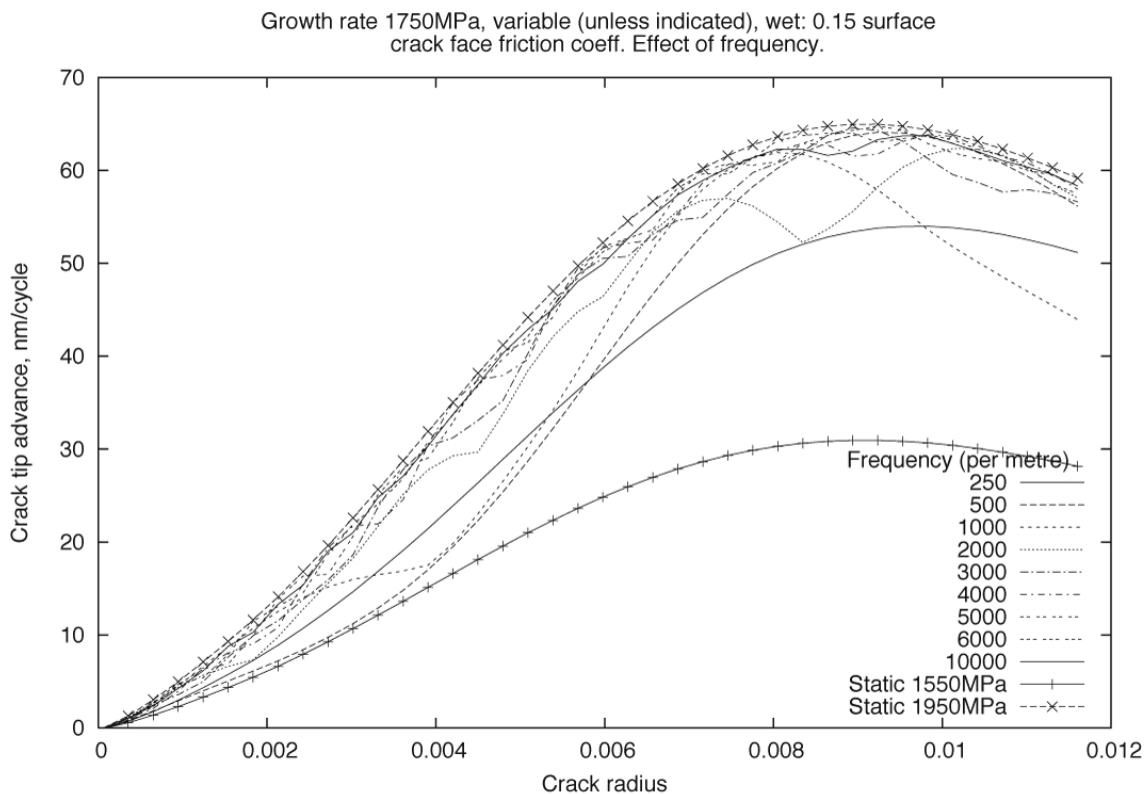


**Figure 37** Effect of frequency on crack growth rate. Frequency is varied for variable 1750MPa pressure, and compared with static 1550MPa and 1950MPa pressures.

## 6.2 The effect of wheel flats on rail breaks

The aim of this part of the study is to establish a scientific foundation for regulations regarding allowed wheel flats. Current wheel removal criteria normally relate the alarm limit to the size (length) of a wheel flat. This is not an optimal situation, partly because of worker's safety: it may be both difficult and dangerous to locate and measure the length of a wheel flat during operations. However, there is also a profound scientific argument against such criteria: a wheel flat of a given size will result in different impact load magnitudes depending on, among other things, the type of vehicle, train speed, axle load and track properties.

Instead the aim of this study is to base the wheel removal criterion on the wheel–rail contact forces, which can be measured by detectors. This leaves us with the question on how the “severity” of an impact load of a certain magnitude should be quantified. In the current study this is related to the risk of rail breaks. This neglects other damage modes, such as sleeper cracking and indentations on the rail surface, etc. However, this was deemed acceptable mainly because rail breaks constitute an immediate safety risk, whereas the other damage modes are more benign in that respect. As shown in the following, the case is extremely complicated even with this limitation.

### 6.2.1 Methodology

To assess the risk of rail breaks, the focus is on “large” cracks in rail heads and rail foots. In the current study “large” head cracks denotes cracks that have deviated to a (more or less) transversal growth path and have grown out of the contact stress field. From a practical perspective this means that the railhead cracks should be larger than about one centimetre. For foot cracks, the restriction is that theories of large crack growth (*i.e.*, mode I propagation and no major interaction with the microstructure) should be valid. This corresponds to a crack size of some millimetres. Under these presumptions, crack growth will mainly be driven by the global bending of the rail. In addition, the thermal loading will have a major effect as will be discussed below.

The next task is to define the relation between an impact load magnitude and the resulting bending moment of a rail. This turns out to be very complicated since the magnitude of the bending moment will depend on a number of parameters. The strategy of the study therefore turned towards defining a “worst-case” wheel flat. To this end, numerical simulations have been employed. These have been validated and calibrated towards full-scale field tests of wheel flat impacts.

To this end, the impact position with respect to the position of the crack was first assessed. For the case of a rail foot crack, it is rather intuitive that the worst combination is a crack in the centre of a sleeper span and a wheel flat impacting directly above the crack. Numerical simulations verified that this was indeed the case. For a rail head crack the case is more complicated. A previous study (Sandström & Ekberg, 2007) has indicated that the worst combination is a rail head crack above a sleeper and a wheel flat impacting one and a half sleeper span away with the two wheels in one bogie on each side of the crack. The current study confirmed this finding for certain cases, but also concluded that in general the situation is more complicated. Depending on the configuration of the track and the vehicle, the worst case could for example be a crack located between two bogies, one of which contains the flatted wheel. Needless to say, the establishment of “worst case impact positions” demanded a multitude of numerical simulations. For this reason a simplified time history of the impact load has been developed. This model has been validated towards the “full” numerical model, which in turn has been validated towards full-scale field tests.

The second parameter with a major influence is the frequency content of the impact load. To establish this influence a full factorial design analysis was employed. In addition, the influence of the most significant parameters was studied more in detail. In addition, results from field tests have been utilized to define realistic limits of the parameter variations.

The analysis should also account for varying vehicle conditions. To this end, three operational conditions that were deemed to be very demanding were selected. These were heavy haul operations at 60 km/h (axle load 30 tonnes), freight operations at 100 km/h (25 tonnes) and passenger traffic at 200 km/h (21 tonnes).

Finally, varying track characteristics need to be accounted for. An initial study has concluded that the ballast stiffness had a significant influence. To quantify this influence, different values of ballast stiffness have been employed in the simulations.

## 6.2.2 Simulations

Under these conditions, a parametric study was carried out and the maximum bending moment in the rail in a sleeper span (to assess fracture of a rail foot crack) and above a sleeper (to assess fracture of a rail head crack) was evaluated. This was carried out for impact loads in the range 250 kN to 350 kN. This range was considered to capture realistic alarm limits based on operational impact load magnitudes.

Setting out from the derived bending moments, the risk of fracture was assessed. To this end, the loading of the crack was quantified by the stress intensity factor. The case is complicated by the fact that in addition to rail bending an all-welded rail is also subjected to a tensile stress due to restricted thermal contraction. This will result in additional stress intensity. However, in contrast to the varying bending stress, the thermal stress is (more or less) constant. By a fracture mechanics analysis, the risk of fracture was assessed for different operational conditions.

In addition, crack growth was evaluated. This called for additional input since crack growth is related to the range of the stress intensity factor (in contrast to fracture, which is related to the maximum magnitude of the stress intensity factor during a wheel passage).

In addition to the study above, the influence of hanging sleeper(s) was assessed. Hanging sleepers are sleepers where the underlying ballast provides very limited support. They will therefore result in locally increased bending moments in the rail due to the locally increased deflection. To define a “worst case” of hanging sleeper(s) turned out to be very cumbersome due to the fact that the influence of hanging sleeper(s) is highly dependent on the impact position, but also on the characteristics of the passing vehicle, etc. Eventually there was success in establishing not only the “worst case”, but also to quantify the influence of a hanging sleeper on the induced bending moments and consequently on the risk of rail breaks and crack growth rates.

## 6.2.3 Conclusions

Details on the simulations and more in-depth conclusions are given in Annexes 4, 5 and 6. The investigation will continue and be reported in the deliverable D4.2.6 where it is foreseen that more explicit guidelines can be given. Below is a summary of the most important conclusions to date from an implementation point of view.

- Critical crack sizes (i.e., crack sizes for which fracture is likely) for rail head and foot cracks depend significantly on the temperature (or rather the temperature below the stress free temperature). For cold conditions, critical crack sizes of roughly 1 and 3 cm are found for rail foot and rail head cracks respectively.
- Crack growth rates are significantly increased close to fracture. Consequently, operationally **allowed** crack sizes need to be much smaller. Exactly how much smaller depends on the accuracy of inspections (i.e., how small cracks can with certainty be detected) and inspection intervals. To guide in this decision, crack growths evaluated for different operational conditions and presented in appendix 6 can be employed.
- A decrease in the assured largest crack size after an inspection (i.e., the size of a crack that with full certainty can be found at an inspection) will have a major influence on the needed length of the inspection intervals.
- Low ballast stiffness will normally lead to higher rail bending moments. To avoid this influence the ballast stiffness per half sleeper should be kept above some 30 MN/m. Hanging sleepers will remove the beneficial effect of high ballast stiffness and should be avoided. In particular this seems to be the case for high-speed operations (200 km/h in the current study).
- It is recommended to combine the mitigation of a hanging sleeper with an inspection for rail head and rail foot cracks.
- The temperature will have a very significant effect on both crack growth rates and risk of final fracture. To this end it is recommended that the magnitude of allowed wheel–rail impact forces be related to the temperature. Further, inspection intervals need to be significantly reduced during cold periods. Guidance in defining alarm limits and inspection intervals can be obtained from the results presented in Annex 6.
- Due to the significant increase in crack growth rates in cold climate it is recommended that there is an inspection before a cold period to minimize the occurrence of larger cracks that may propagate to fracture.
- The wheel–rail impact force will have an effect on the risk of fracture. To establish alarm limits is a balance between allowed forces and allowed crack sizes. Due to this, a higher alarm limit can be allowed if shorter crack sizes are assured (e.g., by more frequent inspections).
- It is wise to introduce multiple alarm levels for several reasons:
  - A wheel that induces a high impact load is likely to cause damage on the vehicle (in the wheel, in the roller bearing, etc.). This may lead to increased costs and operational disturbances.
  - Also wheels that induce impact loads below an alarm limit corresponding to rail breaks may cause smaller, arrested cracks to start growing. In particular this is likely to be an issue for rail head cracks where a higher load may cause a crack to deviate transversally, which eventually may lead to a rail break.
  - The introduction of low-level alarms is likely to give the maintenance organisation improved possibilities of planning and optimising maintenance procedures. If only a one-level alarm exists there is an obvious risk that a vehicle that just passes the limit may fail in a subsequent control where operational conditions are slightly different. This will, obviously, result in unnecessary costs and operational disturbances.
  - For the same reason as outlined above, it is recommended that the low-level alarm limit is gradually decreased over a period before the introduction of “cold climate” alarm limits.

## 7. Conclusions

---

### **Wear-Hardness Correlation**

Four pearlitic rail steels (CORUS 260, CORUS 400, VA 350 and VA 400) were tested against VAS R7 wheel steel. Three twin-disc tests were performed for each rail steel: 5000 cycles dry; 5000 cycles dry followed by 5000 cycles wet (i.e., water-lubricated); and 15000 cycles dry.

A number of observations were made:

- Rail disc wear decreased when rail steel hardness increased.
- In general, the harder the rail disc material becomes at the surface, the harder the wheel disc material becomes at the surface.
- Wheel disc wear in dry tests was highest when running against VA 350.
- Wheel disc wear in dry tests was higher than the corresponding rail disc wear, except for CORUS 260 which had the highest wear rate.
- In wet tests, wheel disc wear rate drops as rail disc hardness increases.
- In the system as a whole (i.e., considering both wheel and rail discs), using harder CORUS 400 and VA 400 rail steels lowers the total wear rate; also, the wear rate did not increase significantly when discs were run from 5000 to 15000 cycles.

From a review of the academic literature, there is no conclusive finding that harder rails wear wheels more, or vice versa. In general, harder materials wear less, but material hardness is not the only determining factor of wear performance; microstructure and strain-hardening behaviour are critical factors, and rolling contact fatigue performance is equally important. However, as a fairly general rule:

→ *To reduce system wear, harder steel grades should be used for both wheel and rail.*

### **Wear Model Development, Calibration and Validation**

The mixed (dry-wet) SUROS tests caused severe rolling contact fatigue, affecting hardness readings and wear rates, but the dry tests have provided an excellent resource for wear model development and calibration. One aim of the tests was to partly calibrate the wear model while leaving the opportunity also to validate it. Therefore, material hardness models were developed and calibrated for all four rail steels, but the wear model itself was calibrated only against CORUS 260, so that wear predictions for the premium grade rail steels could be used for validation.

Test specimens have been sectioned and analysed by taking microhardness measurements and shear strain estimates. Microhardness measurements have suggested a possible softening effect at very small strains, and a new strain-hardening equation is used to fit to the strain-hardness data for each of the four steels. In addition to a new hardening equation, wear model calibration has led to the introduction of a new ratcheting equation, a new 'greyscale' approach to ductility exhaustion and failure, and a new equation for modelling the effect of roughness of the opposite surface.

The wear rate predictions for the premium grade rail steels match measured values (approximately) for the 5000 cycles dry tests, but over-predict the wear rate for the 15000 cycles dry tests by a factor of 2-3. (The dry-wet test predictions do not match, but are not expected to, since the ratcheting wear model does not account for major surface deterioration caused by significant surface cracking.)

→ *Following major development, the wear model has been calibrated successfully for CORUS 260 rail steel under dry contact conditions.*

→ *The wear model has been partly validated for the premium grades. Additional test work and metallurgical analysis should lead to improved material hardening models.*

### **Effect of Vehicle Characteristics: Rail Wear Predictions**

The wear model, calibrated for CORUS 260 and dry contact, was used to study the effect on rail wear of vehicle characteristics through their effect on the wheel-rail contact. The patch was assumed to be elliptical and the pressure distribution to be Hertzian; in addition, the contact was assumed to be on the top the rail, suitable for straight track, not curves, and the traction to be longitudinal only. A new static partial slip model was used to study the effect of traction.

Traction coefficient has a significant effect on the wear rate. For distributed traction systems the traction coefficient may often be about 0.1, i.e., an average wear rate of about 0.75nm/cycle. For locomotives the traction coefficient may be 0.3 or even higher, i.e., an average wear rate of 1.5nm/cycle or more.

This work uses general wheel-rail contacts, but based on the 160 wear simulations performed:

- *There was a very clear linear trend of wear rate against peak contact pressure (for the range of pressures studied).*
- *Wear equations, giving wear rate for a given pressure and traction coefficient, have been extrapolated which can be used for quick estimation of rail wear.*

### **Out-of-Round Wheels**

Wear rate is not affected by wheel-rail contact variation outside the contact patch. Out-of-round wheels causing a short-wavelength (i.e., less than about 20mm) pressure variation will have an effect on the stress cycle experienced by the rail, and could be modelled following some additional development. The effect of longer wavelength pressure variation on rail wear rate can be studied by considering each wheel pass as an independent event. Wear simulations were thus performed by varying the normal load with each passing wheel, and the predictions compared with the constant average-load case. No significant difference was observed.

- *Long-wavelength out-of-round pressure variations do not affect rail wear significantly.*

The effect of periodic variation of wheel-rail contact patch pressure on propagation of semi-circular cracks up to 12mm radius (i.e., penetrating to a depth of about 6mm at 30° angle to the surface) was studied using the '2.5D' Green's-function-based model. The following conclusions were reached:

- *For pressure variations with a wavelength less than about 2mm, the maximum pressure should be used to calculate crack growth rate.*
- *For pressure variations with a wavelength greater than about 20mm, there is no advantage to modelling pressure variation within a single load pass, and that modelling successive wheel passes with different static pressures would be sufficient.*
- *Out-of-round wheels with roughness features between these two wavelengths would accelerate crack propagation, but would require more detailed modelling.*

### **Rail crack growth and rail breaks**

For an analysis of long crack growth and rail breaks numerical simulations validated and calibrated towards full-scale field tests featuring flattened wheels have been employed. The main conclusions from the simulations were the detrimental influence of rail temperature and low ballast stiffness (where hanging sleeper(s) is an extreme case).

The influences of the most important parameters have been quantified. The results are presented in Annexes 4, 5 and 6 and summarized in Section 6.2 where also the conclusions and recommendations for operational guidelines are described.

## 8. Bibliography

---

- Archard, J.F.** (1953) 'Contact and rubbing of flat surfaces.' *Journal of Applied Physics*, 24:981–988.
- Benson, M.** (1993) 'Effect of differential hardness on wheel/rail wear – Literature survey.' British Rail Research, Derby, UK, September.
- Burstow, M., Fletcher, D.I., Franklin, F.J., and Kapoor, A.** (2008) 'Management and understanding of rolling contact fatigue: Mechanisms of crack initiation.' Rail Safety & Standards Board, Project T355 [http://www.rssb.co.uk/pdf/reports/research/T355\\_rpt\\_final\\_wp1.pdf](http://www.rssb.co.uk/pdf/reports/research/T355_rpt_final_wp1.pdf).
- Fletcher, D.I., Franklin, F.J., and Kapoor, A.** (2003) 'Image analysis to reveal crack development using a computer simulation of wear and rolling contact fatigue.' *Fatigue and Fracture of Engineering Materials and Structures*, 26(10):957–967.
- Fletcher, D.I., Kapoor, A., Franklin, F.J., Smith, L., and Hyde, P.** (2006) 'Comparison of the Hatfield and alternative UK rails using models to assess the effect of residual stress on crack growth from rolling contact fatigue.' Health & Safety Laboratory's project JR31.086 <http://www.hse.gov.uk/research/rrpdf/rr461.pdf>.
- Fletcher, D.I., Franklin, F.J., Garnham, J.E., Muyupa, E., Papaelias, M., Davis, C.L., Kapoor, A., Widiyarta, I., Vasić, G.** (2008) 'Three-Dimensional Microstructural Modelling Of Wear, Crack Initiation and Growth In Rail Steel.' Proceedings of the 8th World Congress on Railway Research (WCRR), May 18-22, Soeul, Korea.
- Franklin, F.J., Widiyarta, I., and Kapoor, A.** (2001) 'Computer simulation of wear and rolling contact fatigue.' *Wear*, 250(2):949–955.
- Franklin, F.J., Chung, T., and Kapoor, A.** (2003) 'Ratcheting and fatigue-led wear in rail-wheel contact.' *Fatigue and Fracture of Engineering Materials and Structures*, 26(10):949–955.
- Franklin, F.J., and Kapoor, A.** (2007) 'Modelling wear and crack initiation in rails.' RRUUK Special Issue of the *Proceedings of the IMechE, Part F: Journal of Rail and Rapid Transit*, 221:23–33.
- Franklin, F.J., Garnham, J.E., Fletcher, D.I., Davis, C.L., and Kapoor, A.** (2008) 'Modelling rail steel microstructure and its effect on wear and crack initiation.' *Wear*, 265:1332–1341.
- Garnham, J.E., Franklin, F.J., Fletcher, D.I., Kapoor, A., and Davis, C.L.** (2007) 'Predicting the life of steel rails.' *RRUK Special Issue of the Proceedings of the IMechE, Part F: Journal of Rail and Rapid Transit*, 221:45–58.
- Haines, D.J., and Ollerton, E.** (1963) 'Contact Stress Distributions on Elliptical Contact Surfaces Subjected to Radial and Tangential Forces', *Proceedings of the IMechE*, 177(4):95–114.
- Jendel, T.** (2002) 'Prediction of wheel profile wear-comparisons with field measurements.' *Wear*, 253:89–99.
- Mädler, K., Zoll, A., Heyder, R., and Brehmer, M.** (2008) 'Rail Materials - Alternatives and Limits.' Proceedings of the 8th World Congress on Railway Research (WCRR), May 18-22, Soeul, Korea.
- Kapoor, A.** (1994) 'A re-evaluation of the life to rupture of ductile metals by cyclic plastic strain.' *Fatigue and Fracture of Engineering Materials and Structures*, 17:201–219.
- Kapoor, A., and Franklin, F.J.** (2000) 'Tribological layers and the wear of ductile materials.' *Wear*, 245(1-2):204–215.
- Kapoor, A., Franklin, F.J., Wong, S.K., and Ishida, M.** (2002) 'Surface roughness and plastic flow in rail wheel contact.' *Wear*, 253(1-2):257–264.
- Kapoor, A., Beynon, J.H., Fletcher, D.I., and Loo-Morrey, M.** (2004) 'Computer simulation of strain accumulation and hardening for pearlitic rail steel undergoing repeated contact.' *The Journal of Strain Analysis for Engineering Design*, 39(4):383-396.
- Lee, K.M., and Polycarpou, A.A.** (2005) 'Wear of conventional pearlitic and improved bainitic rail steels.' *Wear*, 259(1-6):391–399.
- Markov, D.** (1995) 'Laboratory tests for wear of rail and wheel steels.' *Wear*, 181-183(Part 2): 678-686.
- Pointner, P.** (2008) 'High strength rail steels – The importance of material properties in contact mechanics problems.' *Wear*, 265(9-10):1373–1379.

- Johan Sandström & Anders Ekberg**, (2007) 'Predicting crack growths and risks of rail breaks due to wheelflat impacts in heavy haul operation's, IHHA Special Technical Session, Kiruna, Sweden, 10 pp
- Sankaran, S., Subramanya Sarma, V., and Padmanabhan, K.A.** (2003) 'Low cycle fatigue behavior of a multiphase microalloyed medium carbon steel: comparison between ferrite/pearlite and quenched and tempered microstructures.' *Materials Science and Engineering*, A345:328–335.
- Sato, M., Anderson, P.M., and Rigney, D.A.** (1993) 'Rolling-sliding behavior of rail steels.' *Wear*, 162-164(1):159–172.
- Singh, U.P., and Singh, R.** (1993) 'Wear investigation of wheel and rail steels under conditions of sliding and rolling-sliding contact with particular regard to microstructural parameters.' *Wear*, 170(1):93–99.
- Tyfour, W.R., Beynon, J.H., and Kapoor, A.** (1995) 'The steady state wear behaviour of pearlitic rail steel under dry rolling-sliding contact conditions.' *Wear*, 180(1-2):79–89.
- Tyfour, W.R., Beynon, J.H., and Kapoor, A.** (1996) 'Deterioration of rolling contact fatigue life of pearlitic rail steel due to dry-wet rolling-sliding line contact.' *Wear*, 197:255–265.
- Vermeulen, P.J., and Johnson, K.L.** (1964) 'Contact of Nonspherical Elastic Bodies Transmitting Tangential Forces', *Trans ASME, J. Appl. Mech.*, 338–340.
- Widiyarta, I., Franklin, F.J., and Kapoor, A.** (2008) 'Modelling thermal effects in ratcheting-led wear and rolling contact fatigue.' *Wear*, 265:1325–1331.
- Zakharov, S.V., Goryachea, I., Bogdanov, V., Pogorelov, D., Zharov, I., Yasikov, V., Torskaya, E., and Soshenkov, S.** (2008) 'Problems with wheel and rail profiles selection and optimisation'. *Wear*, 265:1266–1272.

## 9. Annexes

---

1. INT-SP4-30-090223-D4-SUROS-TWIN-DISC-TEST-RESULTS:  
"SUROS Twin-Disc Test Results"
2. INT-SP42-30-090217-D1-WEAR-SIMULATION-ADDITIONAL-RESULTS:  
"Wear Simulation Additional Results"
3. K. Mädler, A. Zoll, R. Heyder, M. Brehmer, 'Rail Materials - Alternatives and Limits', *WCRR Conference 2008, Korea*.
4. E. Kabo, A. Ekberg, J. C. O. Nielsen, 'Analysis of static fractures of rails due to wheel flats', Research report 2009:01, Department of Applied Mechanics, Chalmers University of Technology, Gothenburg, 2009, 18 pp.
5. J. C. O. Nielsen, E. Kabo, A. Ekberg, 'Alarm limits for wheel-rail impact loads – part 1: rail bending moments generated by wheel flats', Research report 2009:02, Department of Applied Mechanics, Chalmers University of Technology, Gothenburg, 2009, 31 pp.
6. A. Ekberg, E. Kabo, J. C. O. Nielsen, 'Alarm limits for wheel-rail impact loads – part 2: analysis of crack growth and fracture', Research report 2009:03, Department of Applied Mechanics, Chalmers University of Technology, Gothenburg, 2009, 49 pp.